Aus der Klinik und Poliklinik für Diagnostische und Interventionelle Radiologie
der Universitätsmedizin der Johannes Gutenberg-Universität Mainz

Evaluation und Quantifizierung von kardialen Strukturen mittels Photon-counting CT

Inauguraldissertation
zur Erlangung des Doktorgrades der Medizin
der Universitätsmedizin
der Johannes Gutenberg-Universität Mainz

Vorgelegt von

Elias Volker Wolf
aus Heidelberg

Mainz, 2025

Wissenschaftlicher Vorstand: Univ.-Prof. Dr. Philipp Drees

1. Gutachter: Prof. Dr. med. Karl-Friedrich Kreitner

2. Gutachter:

3. Gutachter:

Tag der Promotion: 16.03.2026

In memoriam Opa Günter

Inhaltsverzeichnis

Abkürzungsverzeichnis

CAD-RADS	Coronary Artery Disease Reporting and Data System
CCTA	Koronare CT-Angiografie (Coronary CT Angiography)
EID-CT	Energie-Integrierende Detektor-Computertomografie
ICA	Invasive Koronarangiografie (Invasive Coronary Angiography)
ICC	Intraclass Correlation Coefficient
KHK	Koronare Herzkrankheit
LVM	Linksventrikuläres Myokard
PCD-CT	Photon-Counting Detektor-Computertomografie
PDS	Prozentuale Diameterstenose
QCA	Quantitative Coronary Angiography
QIR	Quantum Iterative Reconstruction
UHR	Ultra-high Resolution
VMI	Virtual Monoenergetic Images
VNCa	Virtual Non-Calcium

1 Zusammenfassung

Erkrankungen des Herzens wie die koronare Herzkrankheit (KHK) treten in unserer Gesellschaft zahlreich auf und gelten derzeit als häufigste Todesursache (1). Daher ist es von Bedeutung, eine möglichst genaue medizinische Diagnostik, Einordnung und daraus resultierende Therapiemöglichkeiten für Patienten anbieten zu können.

Die koronare CT-Angiografie (engl. „Coronary CT Angiography“ (CCTA)) stellt dafür eine der am häufigsten angewandten klinischen Methoden zur Abklärung der stabilen KHK dar (2, 3). Als eine nicht-invasive Methode der Bildgebung ermöglicht die CCTA die Identifizierung chronischer Koronarerkrankungen ohne die Risiken einer invasiven Koronarangiografie (engl. „Invasive Coronary Angiography“ (ICA)). Dies macht sie zu einer sichereren Option für die Herz-Diagnostik, und sie wurde auch bei Verdacht auf eine chronische KHK in den Leistungskatalog der gesetzlichen Krankenkassen im Jahr 2024 aufgenommen. Die Leistungsfähigkeit der CCTA ist aber dabei von unterschiedlichen Untersuchungsmethoden und Einstellungen des CT-Gerätes abhängig.

Mit der Photon-Counting Detektor-Computertomografie (PCD-CT) ist eine fortschrittliche CT-Technologie seit 2021 in der klinischen Routine verfügbar. Im Gegensatz zur konventionellen Energie-Integrierenden Detektor-Computertomografie (EID-CT) ermöglicht die PCD-CT eine direkte Umwandlung von Röntgenquanten in elektrische Signale durch Semikonduktoren. Diese innovative Methode bietet eine höhere räumliche Auflösung, ein reduziertes Bildrauschen und durchgängig verfügbare spektrale Bildinformationen (4-6). Die verbesserte Bildqualität erhöht selbst bei starker Verkalkung die Erkennbarkeit des Koronarlumens und ermöglicht eine präzisere Analyse der Plaquezusammensetzung (7-10). Die durch die PCD-CT bereitgestellten zusätzlichen Informationen könnten möglicherweise die Charakterisierung der Koronararteriensklerose verbessern, was zu präziseren Diagnosen und differenzierteren Therapieempfehlungen für Patienten führt.

Die zentrale Fragestellung dieser Dissertation lautet, ob die neuartige PCD-CT eine verbesserte Evaluation und Quantifizierung von kardialen Strukturen ermöglicht. Dies wurde in unterschiedlichen präklinischen und klinischen Experimenten mit verschiedenen Herz-Untersuchungsmethoden validiert.

1.1 Kalzium-Score

Eine wertvolle Methode, um das Vorhandensein und das Ausmaß von Verkalkungen in den Koronararterien initial zu bewerten, ist die Bestimmung des Kalzium-Scores (11). Die Ermittlung des Kalzium-Scores erfolgt über einen EKG-gesteuerten, kontrastmittelfreien Herz-CT-Scan. Dabei wird sowohl die Fläche als auch die Dichte der nachgewiesenen Verkalkungen berücksichtigt. Der Kalzium-Score dient als zuverlässiger Prädiktor für mögliche

unerwünschte kardiale Ereignisse und wird deshalb genutzt, um das Risiko für Herz-Kreislauf-Erkrankungen einzustufen (12-14). Internationale Leitlinien empfehlen diese Methode als sinnvolle Maßnahme, um das individuelle Risiko besser einzuordnen und dadurch eine verbesserte Therapiemöglichkeit für Patienten durchzuführen (15).

In der Publikation 2.1: „Intra-individual comparison of coronary calcium scoring between photon counting detector- and energy integrating detector-CT: Effects on risk reclassification" wurde in einem intraindividuellen Vergleich der Kalzium-Score und das Kalzium-Volumen zwischen der PCD- und der EID-CT untersucht. Das Kalzium-Volumen wurde mit den physikalischen Volumenangaben (98,2 mm^3, 21,2 mm^3 und 0,8 mm^3) des Herstellers jeweils verglichen. Für diese Fragestellung wurde ein Phantom (in vitro) mit einer standardmäßigen Kalzium-Score CT-Untersuchungstechnik (120 kVp, Schichtdicke/Schichtabstand 3/1,5 mm, Qr36 kernel) mit beiden CT-Geräten gescannt. Die CT-Aufnahmen wurden für die EID-CT mit gefilterter Rückprojektion und für die PCD-CT mit einem monoenergetischen Level von 70 keV und dem ausgeschalteten Quantum Iterative Reconstruction (QIR) off rekonstruiert. Damit wurden möglichst vergleichbare Einstellungen zwischen den beiden CT-Geräten hergestellt. Dieselben CT-Einstellungen sind in einer prospektiven Studienkohorte (in vivo) mit insgesamt 23 Patienten verwendet worden. Die Studie wurde von der lokalen Ethikkommission (Health Insurance Portability and Accountability Act–compliant) genehmigt, und alle Patienten gaben eine schriftliche Einverständniserklärung ab. Diese Patienten erhielten als erstes einen EID-CT-Scan und im Median 5,5 (3,0 – 12,5) Tage später einen PCD-CT-Scan. Eine Regressionsformel wurde aus dem in vitro und in vivo Kalzium-Score Vergleich ermittelt, bei der die EID-CT als klinischer Referenzstandard zu der PCD-CT angesehen wurde. Anschließend wurde diese Formel auf 514 Patienten retrospektiv angewendet, die zwischen Januar und Dezember 2021 einen EID-CT Herz-Scan erhielten. Dadurch wurden sie in eine Risikoklassifizierung eingestuft, als hätten sie sich einer PCD-CT Untersuchung unterzogen. Zur Risikobewertung wurde die Rumberger-Klassifikation angewendet, um den Kalzium-Score in die folgenden Kategorien zu unterteilen: 0, 1–10, 11–100, 101–400 und >400 (16).

In den Phantomexperimenten zeigten sich genauere Kalzium-Volumen Messungen für die PCD-CT verglichen mit der EID-CT (Überschätzung der Referenzwerte des Herstellers: PCD-CT: 66,1 ± 1,6% vs. EID-CT: 77,2 ± 0,5%). Kalzium-$Score_{EID\text{-}CT}$ und Kalzium-$Score_{PCD\text{-}CT}$ lieferten sowohl in vitro (r = 0,99, Intraclass Correlation Coefficient (ICC) = 0,99) als auch in vivo (r = 0,94, ICC = 0,99) eine starke Korrelation zueinander. Dennoch erreichte Kalzium-$Score_{PCD\text{-}CT}$ signifikant niedrigere Ergebnisse in vitro (Kalzium-$Score_{PCD\text{-}CT}$: 60,5 (30,2 – 170,3) vs. Kalzium-$Score_{EID\text{-}CT}$: 74,7 (34,6 – 180,8), p = 0,0015) und nicht-signifikant in vivo (Kalzium-$Score_{PCD\text{-}CT}$: 174,3 (11,1 – 872,7) vs. Kalzium-$Score_{EID\text{-}CT}$: 218,2 (18,5 – 876,4), p = 0,10). Durch die stetig niedrigeren Kalzium-$Score_{PCD\text{-}CT}$ Werte wurden in der simulierten Patientenkohorte 5,25% der Patienten in eine neue, niedrigere Risikoklasse reklassifiziert.

Zusammenfassend korrelierte der Kalzium-Score$_{PCD\text{-}CT}$ sehr stark mit dem Kalzium-Score$_{EID\text{-}CT}$. Zudem erzielte die PCD-CT niedrigere Werte für den Kalzium-Score und das Kalzium-Volumen, was eine mögliche genauere Quantifizierung verglichen mit der EID-CT darstellt.

1.2 **Stenosequantifizierung**

Neben dem Kalzium-Score ist eine genaue CT-basierte Quantifizierung des Stenosegrades und die Ermittlung der prozentualen Diameterstenose (PDS) der Koronararterie von großer Bedeutung. Der PDS-Wert wird dabei auf Höhe der Stenose durch das Verhältnis aus verbleibendem Gefäßdiameter zum mittleren Koronargefäßdurchmesser bestimmt. Die Bestimmung der PDS-Werte erfolgt nach der gleichen Methode wie die Messung des Stenosegrades im Herzkatheterlabor und wird daher auch in den Society of Cardiovascular Computed Tomography-Richtlinien empfohlen (17). Dies stellt die Voraussetzung zur Risikobewertung der KHK und der daraus resultierenden Therapieempfehlung dar (18, 19). Ein Nachteil der konventionellen CT-Bildgebung ist aber die Überschätzung des Stenosegrades im Vergleich zur ICA, insbesondere beim Vorliegen vieler Kalzifikationen der Koronararterien (20). Diese Überbewertung wird vorwiegend durch Kalzium-Blooming-Artefakte hervorgerufen (4). Aufgrund dieser Überbewertung besteht das Risiko, dass an Patienten, die eigentlich keine klinisch relevante Stenose aufweisen, dennoch ICA-Untersuchungen durchgeführt werden (21).

Die Publikation 2.2: „Intra-individual comparison of coronary artery stenosis measurements between energy-integrating detector CT and photon-counting detector CT" erörtert, inwiefern die PCD-CT verglichen mit der EID-CT die Stenosequantifizierung beeinflusst. Für diese Fragestellung sind CCTA-Aufnahmen mit der PCD- und der EID-CT in einer prospektiven Studienkohorte mit 23 Patienten, genehmigt durch die lokale Ethikkommission, angefertigt worden. Die CCTA-Aufnahmen wurden vergleichbar zueinander rekonstruiert (EID-CT: Bv36 kernel, 110 kVp, Schichtdicke 0,5 mm, Admire 3, PCD-CT: Bv36 kernel, 120 kVp, Schichtdicke 0,6 mm, QIR 3, 55keV). Für alle Scans wurde ein prospektiv getriggertes sequentielles Herzprotokoll im sogenannten „Step & Shoot"-Modus mit EKG-Triggerung verwendet. Aus den Patientenuntersuchungen wurden 42 kalzifizierte Plaques für die weitere Analyse identifiziert. Zwei Beurteiler bewerteten diese Plaques hinsichtlich ihres PDS-Wertes und der daraus resultierenden Coronary Artery Disease Reporting and Data System (CAD-RADS) – 2.0 Klassifizierung (18).

Die PCD-CT lieferte im Median niedrigere PDS-Ergebnisse verglichen mit der EID-CT (PDS$_{EID\text{-}CT}$: 45,1% (35,1% – 64,0%) vs. PDS$_{PCD\text{-}CT}$: 44,2% (32,4% – 61,0%), $p < 0{,}0001$). Trotzdem korrelierten die beiden Messungen sehr stark (ICC = 0,99) miteinander. Durch die tendenziell niedrigeren PDS-Werte in der PCD-CT ergab sich ein intraindividueller Messunterschied von 1,8% zwischen den beiden CT-Scannern. Daraus folgte in einer pro-Patienten-Analyse eine

Re-Klassifizierung in 3/23 Patienten (13,0% neue, niedrigere Klasse) für den ersten Beurteiler und in 4/23 Patienten (13,0% neue, niedrigere und 4,4% neue, höhere Klasse) für den zweiten Beurteiler. Die beiden Beurteiler erzielten eine hohe Übereinstimmung in der PDS-Quantifizierung (ICC = 0,98).

Grundsätzlich zeigte sich bei vergleichbarer Rekonstruktion eine hohe Korrelation in der Stenosequantifizierung zwischen der PCD- und der EID-CT. Dadurch ist die neuartige PCD-CT der EID-CT als gleichwertig anzusehen und für die klinische Routine anwendbar. Mit der PCD-CT wurden tendenziell kleinere Stenosewerte gemessen, was letztendlich zu einer Re-Risikoklassifizierung und entsprechenden Empfehlungen für das folgende diagnostische und therapeutische Management von 17,4% der Patienten führte.

Dies allein würde aber nicht die gegenwärtigen Limitationen der EID-CT Technologie überwinden. Eine PCD-CT spezifische Möglichkeit, um die Genauigkeit der CCTA zu verbessern, besteht darin, Virtual Monoenergetic Images (VMI) bei hohen Energiestufen zu rekonstruieren (22, 23). Dadurch können die Bildeffekte des Kalzium-Bloomings minimiert und die Genauigkeit der Stenosebestimmung erhöht werden. Die genaue PDS-Bestimmung durch die CCTA ist entscheidend, da die Schwere der Stenose in Kombination mit dem Kalzium-Score eine wichtige Grundlage für die klinische Entscheidungsfindung bietet.

Das Ziel der Publikation 2.3: „Photon-Counting Detector CT Virtual Monoenergetic Images for Coronary Artery Stenosis Quantification: Phantom and In Vivo Evaluation” besteht darin, die Auswirkungen verschiedener VMI Level auf die Genauigkeit von CCTA-Stenosemessungen mittels der PCD-CT zu untersuchen. Dies wurde sowohl anhand eines dynamischen Phantoms als auch an einer Patientengruppe mit ICA durchgeführt.

An dem dynamischen Phantom, welches eine 25% und eine 50% kalzifizierte Stenose aufweist, erfolgten PCD-CT-Aufnahmen (120 kvP, QIR 3, Qr40, Schichtdicke 0,4 mm), sowohl ohne als auch mit simulierten Herzbewegungen (0, 50, 60, 70 und 80 Schläge/min). Alle Aufnahmen wurden mit prospektiver EKG-Triggerung bei 30% bis 80% des R-R Intervalls durchgeführt. Die CT-Scans wurden in 9 verschiedenen VMI-Stufen (40 – 140 keV) rekonstruiert. Zusätzlich wurden 33 Patienten (7 weiblich, 26 männlich; 71,3 ± 9,0 Jahre) mit 64 Plaques (37 kalzifizierte, 18 gemischte und 9 nicht-kalzifizierte Plaques) in einer retrospektiven Analyse identifiziert und unter identischen CT-Einstellungen rekonstruiert. Diese Patienten unterzogen sich innerhalb ihrer medizinischen Behandlung im Anschluss an die CCTA einer klinisch indizierten ICA. Die PDS-Werte wurden jeweils daraus ermittelt und mit den Referenzwerten des Phantomherstellers bzw. mit den Quantitative Coronary Angiography (QCA)-Messungen aus den ICAs in der Studienkohorte verglichen. Zusätzlich wurden Bloomingartefakte in den kalzifizierten und gemischten Plaques bestimmt.

In beiden Experimentteilen konnte gezeigt werden, dass sich mit steigendem VMI Level die PDS- und Blooming-Werte kontinuierlich verringerten. Im Phantom lieferten 90 keV (bias, 1,4%) bei der 25% Stenose und 100 keV (bias, -0,4%) bei der 50% Stenose die geringsten Abweichungen zu den Referenzwerten. In der Patientenkohorte ergaben sich die besten Übereinstimmungen der PDS-Werte mit den QCA-Messungen für kalzifizierte Plaques bei 100 keV (bias, 17,2%), für gemischte Plaques bei 140 keV (bias, 5,0%) und für nicht-kalzifizierte Plaques bei 40 keV (bias, -0,5%).

Dadurch erschließt sich, dass VMI Level die Genauigkeit von PDS-Messungen in der PCD-CT beeinflussen. Die Verwendung spezifischer VMI Level kann die PDS-Quantifizierung für verschiedene Plaquetypen verbessern.

1.3 Texturanalyse des Myokards

Auch die Generierung von Radiomics-Merkmalen stellt eine Möglichkeit dar, quantitative Daten aus verschiedenen diagnostischen Verfahren zu gewinnen (24, 25). Ziel von Radiomics ist es, mittels fortschrittlicher Algorithmen quantitative Merkmale, die für das menschliche Auge schwer zu identifizieren sind, aus medizinischen Bildern zu extrahieren und diese anschließend zu charakterisieren. Diese Daten können genutzt werden, um die Entscheidungsfindung im klinischen Alltag zu unterstützen und zu verbessern. Es konnte gezeigt werden, dass verschiedene VMI-Rekonstruktionen die Eigenschaften von Radiomics-Merkmalen signifikant beeinflussen und dadurch die Reproduzierbarkeit der Radiomics-Daten eingeschränkt wird (26).

In der Studie 2.4: „Photon-counting detector CT-based virtual monoenergetic reconstructions: repeatability and reproducibility of radiomics features of an organic phantom and human myocardium” wurde der Einfluss verschiedener VMI Level auf die Stabilität von Radiomics-Merkmalen in einem Phantom und einer Patientenkohorte untersucht. Das Phantom bestand aus 12 Proben (4 Orangen, 4 Zwiebeln und 4 Äpfeln) und wurde mit einer PCD-CT jeweils fünfmal gescannt (120 kvP, QIR 3, Qr36, Schichtdicke 0,6 mm). In der Studienkohorte wurden 23 Patienten eingeschlossen, die einen PCD-CT-Scan erhielten und mit denselben CT-Einstellungen rekonstruiert worden sind. Zusätzlich wurden 6 verschiedene VMI Level (40, 55, 70, 90, 120 und 190 keV) verwendet. Das Phantom und das linksventrikuläre Myokard (LVM) der Patienten wurden für alle Rekonstruktionen segmentiert. Daraus wurden schließlich 93 Radiomics-Merkmale extrahiert und hinsichtlich ihrer Wiederholbarkeit und Stabilität zwischen den unterschiedlichen VMI Leveln analysiert.

Die Radiomics-Merkmale zeigten in den 5 Phantomscans eine herausragende Wiederholbarkeit (ICC = 1,00). Zwischen den verschiedenen VMI Leveln blieben einige Radiomics-Merkmale unverändert (38,7% in Äpfeln, 30,1% in Orangen und 35,5% in

Zwiebeln). Für das LVM zeigte sich eine Stabilität der Merkmale bei hohen VMI Leveln ≥ 90 keV (90 vs. 120 keV: 77,4%; 90 vs.190 keV: 83,9%; 120 vs. 190 keV: 89,3%). Hingegen bei niedrigeren VMI Leveln resultierten weniger reproduzierbare Radiomics-Merkmale (40 vs. 55 keV: 8,6%).

Zusammenfassend zeigte sich, dass die Stabilität der Radiomics-Merkmale in einem organischen Phantom und im LVM der Patienten stark von den jeweiligen VMI Leveln abhängt. Unterschiedliche spektrale Rekonstruktionen beeinflussen die Radiomics-Merkmale sowohl in vitro als auch in vivo signifikant, was eine Standardisierung der Rekonstruktionsparameter vor der klinischen Anwendung erforderlich macht.

Die PCD-CT ermöglicht eine signifikante Verbesserung der kardiovaskulären CT-Diagnostik in verschiedenen Anwendungen. Dies äußert sich in einer präziseren Bewertung des Kalzium-Scores und einer genaueren Quantifizierung von Stenosen im Vergleich zur konventionellen EID-CT. Darüber hinaus haben unterschiedliche VMI Level sowohl Auswirkungen auf die Genauigkeit der Stenosemessungen als auch auf die Reproduzierbarkeit von Radiomics-Merkmalen.

2 Publikationen

2.1 „Intra-individual comparison of coronary calcium scoring between photon counting detector- and energy integrating detector-CT: Effects on risk reclassification”

Dieses Kapitel basiert auf der bereits veröffentlichten Open-Access-Publikation:

Wolf EV, Halfmann MC, Schoepf UJ, Zsarnoczay E, Fink N, Griffith JP 3rd, Aquino GJ, Willemink MJ, O'Doherty J, Hell MM, Suranyi P, Kabakus IM, Baruah D, Varga-Szemes A, Emrich T. Intra-individual comparison of coronary calcium scoring between photon counting detector- and energy integrating detector-CT: Effects on risk reclassification. Front Cardiovasc Med. 2023 Jan 19;9:1053398. doi: 10.3389/fcvm.2022.1053398.

frontiers | Frontiers in Cardiovascular Medicine

TYPE Original Research
PUBLISHED 19 January 2023
DOI 10.3389/fcvm.2022.1053398

OPEN ACCESS

EDITED BY
Erhan Tenekecioglu,
University of Health Sciences, Türkiye

REVIEWED BY
Rodrigo Salgado,
Antwerp University Hospital & Holy Heart Lier, Belgium
Hengyong Yu,
University of Massachusetts Lowell, United States

*CORRESPONDENCE
Tilman Emrich
Tilman.Emrich@unimedizin-mainz.de

†These authors have contributed equally to this work and share first authorship

SPECIALTY SECTION
This article was submitted to Cardiovascular Imaging, a section of the journal Frontiers in Cardiovascular Medicine

RECEIVED 25 September 2022
ACCEPTED 28 December 2022
PUBLISHED 19 January 2023

CITATION
Wolf EV, Halfmann MC, Schoepf UJ, Zsarnoczay E, Fink N, Griffith JP III, Aquino GJ, Willemink MJ, O'Doherty J, Hell MM, Suranyi P, Kabakus IM, Baruah D, Varga-Szemes A and Emrich T (2023) Intra-individual comparison of coronary calcium scoring between photon counting detector- and energy integrating detector-CT: Effects on risk reclassification. *Front. Cardiovasc. Med.* 9:1053398. doi: 10.3389/fcvm.2022.1053398

Intra-individual comparison of coronary calcium scoring between photon counting detector- and energy integrating detector-CT: Effects on risk reclassification

Elias V. Wolf[1,2†], Moritz C. Halfmann[1,3†], U. Joseph Schoepf[2], Emese Zsarnoczay[2,4], Nicola Fink[2,5], Joseph P. Griffith III[2], Gilberto J. Aquino[2], Martin J. Willemink[6,7], Jim O'Doherty[2,8], Michaela M. Hell[9], Pal Suranyi[2], Ismael M. Kabakus[2], Dhiraj Baruah[2], Akos Varga-Szemes[2] and Tilman Emrich[1,2,3]*

[1]Department of Diagnostic and Interventional Radiology, University Medical Center of the Johannes Gutenberg-University, Mainz, Germany, [2]Division of Cardiovascular Imaging, Department of Radiology and Radiological Science, Medical University of South Carolina, Charleston, SC, United States, [3]German Centre for Cardiovascular Research, Partner Site Rhine-Main, Mainz, Germany, [4]MTA-SE Cardiovascular Imaging Research Group, Medical Imaging Center, Semmelweis University, Budapest, Hungary, [5]Department of Radiology, University Hospital Munich, LMU Munich, Munich, Germany, [6]Department of Radiology, Stanford University School of Medicine, Stanford, CA, United States, [7]Segmed, Inc., Palo Alto, CA, United States, [8]Siemens Medical Solutions USA, Inc., Malvern, PA, United States, [9]Department of Cardiology, University Medical Center of the Johannes Gutenberg-University, Mainz, Germany

Purpose: To compare coronary artery calcium volume and score (CACS) between photon-counting detector (PCD) and conventional energy integrating detector (EID) computed tomography (CT) in a phantom and prospective patient study.

Methods: A commercially available CACS phantom was scanned with a standard CACS protocol (120 kVp, slice thickness/increment 3/1.5 mm, and a quantitative Qr36 kernel), with filtered back projection on the EID-CT, and with monoenergetic reconstruction at 70 keV and quantum iterative reconstruction off on the PCD-CT. The same settings were used to prospectively acquire data in patients (n = 23, 65 ± 12.1 years), who underwent PCD- and EID-CT scans with a median of 5.5 (3.0–12.5) days between the two scans in the period from August 2021 to March 2022. CACS was quantified using a commercially available software solution. A regression formula was obtained from the aforementioned comparison and applied to simulate risk reclassification in a pre-existing cohort of 514 patients who underwent a cardiac EID-CT between January and December 2021.

Results: Based on the phantom experiment, $CACS_{PCD-CT}$ showed a more accurate measurement of the reference CAC volumes (overestimation of physical volumes: PCD-CT 66.1 ± 1.6% vs. EID-CT: 77.2 ± 0.5%). $CACS_{EID-CT}$ and $CACS_{PCD-CT}$ were strongly correlated, however, the latter measured significantly lower values in the phantom ($CACS_{PCD-CT}$: 60.5 (30.2–170.3) vs $CACS_{EID-CT}$ 74.7 (34.6–180.8), p = 0.0015, r = 0.99, mean bias −9.7, Limits of Agreement (LoA) −36.6/17.3) and in patients (non-significant) ($CACS_{PCD-CT}$: 174.3 (11.1–872.7) vs $CACS_{EID-CT}$ 218.2 (18.5–876.4), p = 0.10, r = 0.94, mean bias −41.1, LoA −315.3/232.5). The systematic

lower measurements of Agatston score on PCD-CT system led to reclassification of 5.25% of our simulated patient cohort to a lower classification class.

Conclusion: $CACS_{PCD-CT}$ is feasible and correlates strongly with $CACS_{EID-CT}$, however, leads to lower CACS values. PCD-CT may provide results that are more accurate for CACS than EID-CT.

KEYWORDS

coronary artery calcium scoring (CACS), coronary artery disease, photon-counting detector computed tomography, risk stratification, energy-integrating detector computed tomography

1. Introduction

Coronary artery calcium scoring (CACS) is an established method to assess the presence and extent of coronary artery calcifications (1). CACS is an integral part of several guidelines for risk assessment of coronary artery disease (CAD) in asymptomatic and symptomatic individuals (2, 3).

Recently, a first-generation dual-source photon-counting detector (PCD) computed tomography (CT) with electrocardiogram (ECG) gating capability became clinically available. Compared to conventional energy-integrating detector (EID) CT, PCD-CT directly converts x-ray photons into an electrical signal without a conversion into light. This difference leads to potential advantages of PCD-CT in relation to spatial resolution and image noise. As the PCD-CT detector "counts" each individual photon in relation to its energy, it is thus capable of providing spectral image information for every acquired scan (4). CACS has been investigated in phantom studies using PCD-CT against EID-CT, combining specific settings of different slice thicknesses, quantum iterative reconstruction (QIR) levels, and virtual monoenergetic image (VMI) reconstruction levels (5, 6). However, to the best of our knowledge, no data exists comparing intra-individual CACS between EID- and PCD-CT in patients according to the Agatston standard. In addition, the effect of PCD-CT-based CACS on reclassification rates for risk prediction is unknown.

Hence, the aim of this study was to compare CACS between PCD-CT and conventional EID-CT in a commercially available phantom with known plaque volumes and calcium densities, as well as in a prospective patient cohort. A further aim was to evaluate the possible effects of PCD-CT-based CACS on reclassification of cardiovascular risk.

2. Materials and methods

2.1. Phantom study

A commercially available chest phantom with a cardiac calcification insert (Thorax & Cardiac Calcification Phantom, QRM, Moehrendorf, Germany) was used as the ground truth for the *in vitro* study. The phantom contains nine different cylinders with predefined plaque diameter (small: 1 mm; medium: 3 mm; and large: 5 mm), each with three different densities (low-density: 200 mg/cm^3; medium-density: 400 mg/cm^3, and high-density: 800 mg/cm^3 calcium hydroxyapatite). The thoracic phantom simulates a small-sized patient (anterior posterior and lateral diameter: 200 and 300 mm) and was used without extension rings.

2.2. Phantom data acquisition

Phantom measurements were performed on both a conventional EID-CT (SOMATOM Force, Siemens Healthineers, Forchheim, Germany) and a PCD-CT system (NAEOTOM Alpha, Siemens Healthineers). The PCD-CT contains two photon-counting cadmium telluride (CdTe) detectors with 144 × 0.4 mm collimation on each detector, allowing spectral CT data acquisition at a maximum temporal resolution of 66 ms. The EID-CT is equipped with a detector collimation of 192 × 0.6 mm. For both systems, tube voltage was set to 120 kVp and volumetric CT Dose Index ($CTDI_{vol}$) was matched between the CT systems at 1.5 mGy. ECG signal was simulated at 60 beats per minute and the examination was triggered at the diastolic phase (75% of the cardiac cycle). To account for variability of the different scans, phantom measurements were repeated five times with a 2 mm shift and a 2° rotation (7).

A standard CACS CT protocol in sequential mode with a slice thickness of 3 mm, increment of 1.5 mm and a quantitative kernel (Qr36) was used on both systems. Images were reconstructed using filtered back projection on the EID-CT. For the PCD-CT, CACS scans were acquired according to a protocol suggested by the manufacturer with a monoenergetic reconstruction at 70 keV and the lowest available level of quantum iterative reconstruction (QIR off). Detailed acquisition and reconstruction parameters are listed in **Table 1**.

2.3. Patient study

The protocol of this prospective, HIPAA-compliant, study was approved by the local Institutional Review Board and written informed consent was obtained from all subjects. All patients underwent standard of care imaging on an EID-CT system, and an additional research CT scan on a PCD-CT system between August 2021 and March 2022. The following inclusion criteria were applied: (1) clinical indication for cardiac imaging, and (2) >18 years of age. Exclusion criteria was: unable to be consented.

2.4. Patient data acquisition

CACS scans were acquired according to the phantom experiment using the same two CT systems. $CTDI_{vol}$ were adjusted to be as

10.3389/fcvm.2022.1053398

similar as possible between PCD-CT and EID-CT, and based on the automatic dose selection of the patient at the EID-CT (CareDose4D, Siemens Healthineers). Reconstruction parameters were identical to the phantom experiment.

2.5. Calcium scoring

In vitro and *in vivo* CACS was performed using a commercially available software solution (CT CaScoring, syngo.via Version VB60, Siemens Healthineers) by a single reader with 2 years of experience in cardiovascular radiology, under the supervision of a board-certified cardiovascular radiologist with 12 years of experience. The reader was blinded to the origin of the CACS image. The software solution semi-automatically quantifies coronary artery calcium (CAC) volumes and CACS according to Agatston's method. The algorithm uses a threshold of 130 HU at 120 kVp and a minimum of a 0.5 mm^2 connected area to detect calcium-containing voxels (8). Segments with stents, or affected by artifacts related to pacemakers, or other metallic objects, were manually excluded. Representative phantom and patient examples are given in **Figures 1**, **2**. For risk assessment, the Rumberger classification was used to stratify CACS into the following classes: 0, 1–10, 11–100, 101–400, and >400 (9).

TABLE 1 CT acquisition and reconstruction parameter.

Modality	EID-CT	PCD-CT
Tube potential (kVp)	120	120
Monoenergetic level (keV)	n/a	70
Reconstruction technique	Filtered back-projection	QIR off
Reconstruction kernel	Qr36f	Qr36f
Slice thickness/Increment (mm)	3/1.5	3/1.5
Field of view (mm)	200	200
Matrix size	512 × 512	512 × 512

QIR, quantum iterative reconstruction.

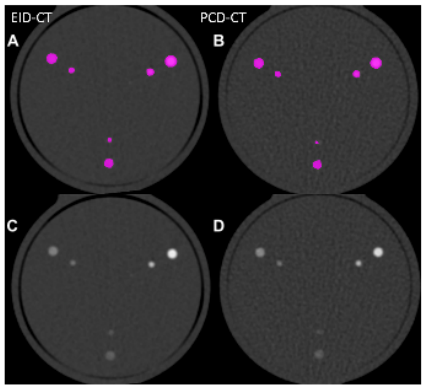

FIGURE 1
Image examples from phantom scanned in the EID-CT **(A,C)** and PCD-CT **(B,D)** with and without color-overlay for CACS.

2.6. Reclassification simulation

A regression model was generated based on the CACS comparison derived from the patient and phantom data to facilitate a virtual recalculation and reclassification in a simulation study as described previously (10). PCD-CT and EID-CT were compared, and the EID-CT was considered as the clinical reference standard. Therefore, a zero value in the EID-CT also causes a non-detectable value in the PCD-CT and there are no negative Agatston scores. Thus, a linear trend line with a y-intercept of zero was fitted to describe inter-scanner CACS differences. A retrospective patient cohort, who had previously undergone cardiac imaging on the same EID-CT between January and December 2021, was used to investigate the effect on the reclassification rate in a larger cohort. Inclusion criteria were an Agatston score above zero. Hence, a total of 514 out of 1,301 screened patients were included in the simulation study.

2.7. Statistical analysis

Statistical analysis was performed using dedicated software (SPSS Statistics for Windows, Version 21.0, IBM Corp Armonk, NY, and MedCalc for Windows, version 15.0, MedCalc Software, Ostend, Belgium). Mean ± standard deviations (SD) were used for normally distributed and median with an interquartile range for non-normal distributed data. Categorical variables are reported with frequencies and proportions. The difference between the CT measurements were compared with the Wilcoxon rank sum tests. A p-value ≤ 0.05 was considered significant. Spearman correlation coefficient (r) was used to assess the correlation between CACS by PCD-CT and EID-CT. Through Bland-Altman analyses, the mean bias, and the upper and lower limits of agreement (LoA) between the two CT techniques were assessed. Intraclass correlations coefficients (ICC) were used to measure the agreement between the two different CT scanners with the following interpretation: 0.0–0.3, lack of agreement; 0.31–0.5, weak agreement; 0.51–0.7, moderate agreement; 0.71–0.9, strong agreement; and 0.91–1.00, very strong agreement (11).

3. Results

3.1. Phantom study

$CACS_{PCD-CT}$ showed a strong correlation to $CACS_{EID-CT}$, however, $CACS_{PCD-CT}$ measured significantly lower values compared to $CACS_{EID-CT}$ ($CACS_{PCD-CT}$: 60.5 (30.2–170.3) vs $CACS_{EID-CT}$ 74.7 (34.6–180.8), p = 0.0015, r = 0.99, ICC = 0.99, mean bias −9.7, LoA −36.6/17.3) (**Figure 3**). Compared to the physical volumes of the calcium inserts, PCD-CT had a lower overestimation to the reference value (overestimation of PCD-CT: 66.1 ± 1.6% vs EID-CT: 77.2 ± 0.5%) (**Figure 4**).

3.2. Patient study

The study population consisted of 23 patients (65 ± 12.1 years) including 16 men and 7 women who underwent CACS scans on both CT scanners. The EID-CT scan was followed by the PCD-CT scan after a median of 5.5 (3.0–12.5) days. Radiation dose (CTDIvol) was

10.3389/fcvm.2022.1053398

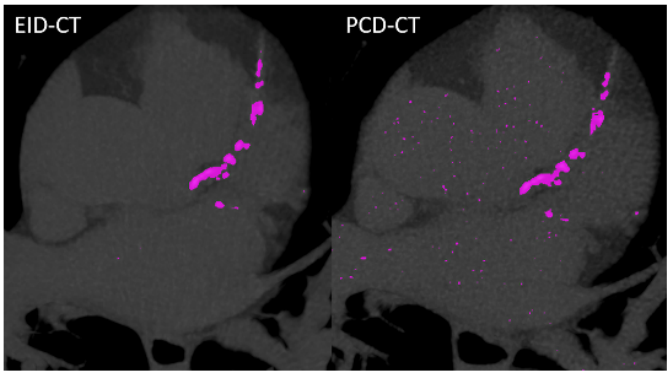

FIGURE 2
Case example from a patient scanned in the EID-CT ($CACS_{EID-CT}$: 964.1) and PCD-CT ($CACS_{PCD-CT}$: 949.9).

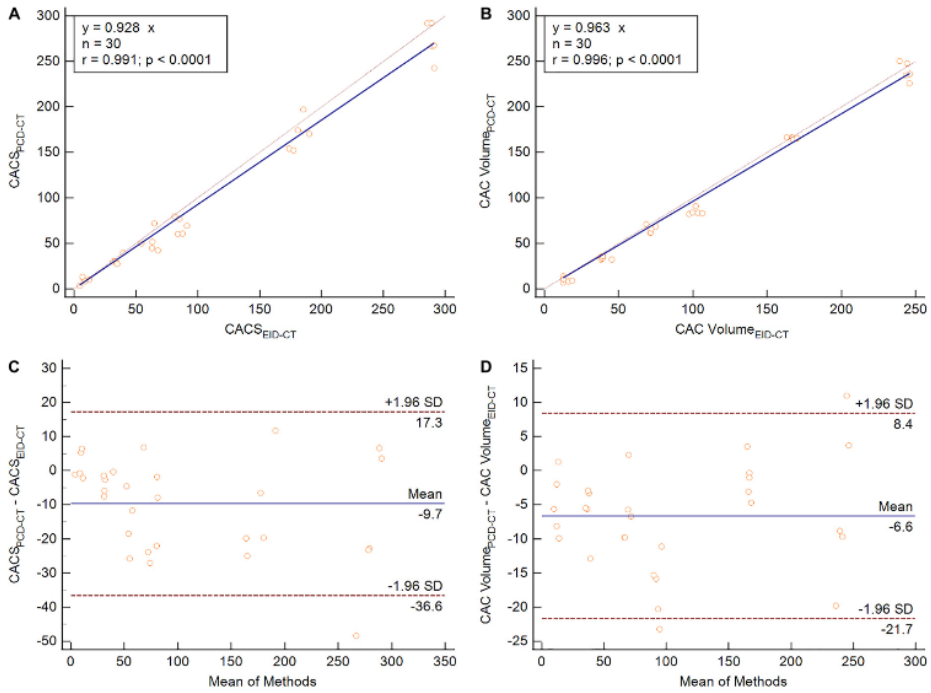

FIGURE 3
Phantom study comparing CACS **(A,C)** and CAC volume **(B,D)** between PCD-CT and EID-CT in scatter- **(A,B)** and Bland-Altman plots **(C,D)**. SD, standard deviation; *r*, Spearmen correlation.

lower in PCD-CT imaging compared to the EID-CT ($CTDI_{vol}$ 2.4 (1.5–3.1) mGy and 2.9 (1.7–3.1) mGy, $p = 0.0001$). Details of the study population are given in Table 2.

Similar to the phantom studies, the *in vivo* comparison yielded strong correlation between PCD-CT and EID-CT for CACS ($r = 0.94$, ICC = 0.99). When comparing median CACS, PCD-CT showed lower CACS then EID-CT, but did not meet statistical significance ($CACS_{PCD-CT}$: 174.3 (11.1–872.7) vs $CACS_{EID-CT}$ 218.2 (18.5–876.4), $p = 0.10$, mean bias −41.1, LoA −315.3/232.5) (Figure 5). Global CACS volume was significantly lower for PCD-CT ($p = 0.04$).

10.3389/fcvm.2022.1053398

Detailed comparisons for the entire heart and per vessel are shown in Table 3.

3.3. Reclassification simulation

The regression equation from *in vitro* and *in vivo* CACS comparison ($CACS_{PCD-CT}$ vs. $CACS_{EID-CT}$; $y = 0.936x$) was used to calculate a new risk classification for PCD-CT. From 1,301 patients, 787 patients had an Agatston score of 0 and 514 patients an Agatston score above zero. From these 514 patients, 5.25% (27 patients) were reclassified in a new, lower CACS risk score classification. Details are provided in Table 4.

4. Discussion

In this study, we investigated the intra-individual difference in CACS between PCD- and EID-CT in a phantom and a patient cohort.

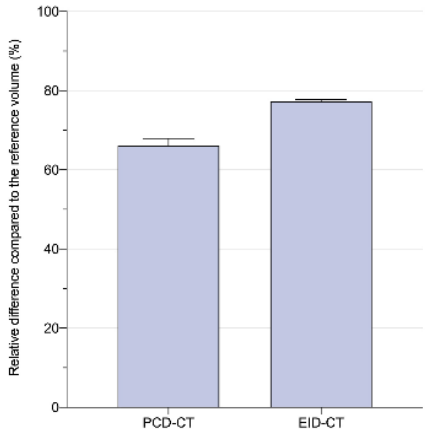

FIGURE 4
Relative difference to the physical calcium insert volume (in percent) for PCD- and EID-CT: 66.1 ± 1.6 vs. 77.2 ± 0.5%.

TABLE 2 Patient characteristics.

	EID-CT	PCD-CT
N	23	
Female (%)	7 (30.4)	
Age (years)	65 ± 12.1	
BMI (kg/m^2)	28.6 (26.7–31.3)	
Difference between both scans (days)	5.5 (3.0–12.5)	
Heart rate (bpm)	66.6 ± 14.5$^{\#}$	62.0 (55.0–73.0)$^{\#}$
$CTDI_{vol}$ (mGy)	2.9 (1.7–3.1)*	2.4 (1.5–3.1)*
DLP (mGy*cm)	45.0 (33.3–61.0)*	33.4 (24.4–48.5)*

Values are mean ± standard deviation, median (interquartile range), absolute and relative frequencies.
BMI, body mass index; CTDI, computed tomography dose index; DLP, dose length product.
Comparison between EID- and PCD-CT: $^{\#}p = 0.82$, $^{*}p < 0.001$.

The major findings are: First, PCD-CT measures lower CACS values compared to EID-CT in an intra-individual *in vitro* and *in vivo* comparison. Second, *in vitro* experiments demonstrated that PCD-CT resulted in more accurate quantification of calcium volume. Third, the reclassification rate for risk prediction was 5.25% using a simulation study of 514 patients who underwent a CACS EID-CT examination.

Various histopathological studies have shown a relevant correlation between coronary calcifications and arteriosclerotic disease (12, 13). CACS has a high negative predictive value, which carries along a low risk for cardiovascular diseases (14, 15). Hence, CACS is a useful diagnostic tool to stratify patients into low and intermediate/high-risk groups. Furthermore, CACS can be used as a prognostic tool predicting cardiovascular events and death (16, 17).

Our results from the phantom study suggest that PCD-CT measures coronary artery calcium (CAC) more accurate than EID-CT. Overestimation of CAC volumes compared to the ground-truth is a widely known phenomenon. For example, van der Werf et al. measured higher CACS values in a phantom using an EID-CT compared to a prototype PCD-CT (6). An overestimation up to 150% of the CAC volume was measured for the large-volume and high-density calcium insert. This overestimation is caused by blooming artifacts that increase the measurable size of plaques (18). Intrinsically, measurements with the PCD-CT system seem to benefit from a reduction of blooming artifacts, even when reconstructed identically to the Agatston standard method derived from EID-CTs. Similarly to phantom experiments that demonstrate lower CACS by PCD-CT compared to EID-CT, our *in vivo* study also produced lower CACS values, despite not being statistically significant, ($p = 0.10$), which may be caused by our small patient sample. These results indicate that PCD-CT derived CACS is more accurate than EID-CT derived CACS with reference to the physical calcification volume.

Other investigations have compared CACS derived by PCD-CT using different settings: Eberhard et al. found that the settings of 70 keV and QIR off; 65 keV and QIR 3/QIR4; Polychromatic images (T3D) at 120 kV and QIR 4 have a <1% deviation from the reference CACS value (5). Additionally, other scan modes such as Sn100 kV with 70 keV and QIR 1 or at 90 kV with 65 keV and QIR 4 could be used to obtain CACS with similar accuracy to the EID-CT and lower radiation dose levels. (19, 20). Furthermore, CACS has also been successfully derived from CCTA datasets by using a novel virtual non-iodine reconstruction (PureCalcium) with high agreement to the true non-contrast acquisition (21).

Despite its clinical and prognostic relevance, CACS is prone to certain limitations (22). One of those is the limited repeatability of CACS on different CT systems, as demonstrated by Willemink et al. in cadaveric hearts (10). Reclassification rate may reach up to 6.5% of cases, depending on the vendor of the CT system. In addition, a certain inter-scan variability also exists when using a CT system for repeated measurements (23). This can be caused by several factors including partial volume effects, different breath-hold depth, and heart rate variability (24). Budoff et al. demonstrated a variability of 11.8% of the Agatston score in patients with end-stage renal disease, especially those with an Agatston score below 30 (inter-scan variability up to 61.3%).

The results of this study demonstrated a ~5% lower CACS derived by PCD-CT compared to EID-CT. This inter-system deviation is in the range of prior reported inter-scan variabilities and indicates that PCD-CT can be used for CACS in clinical routine (23). However, our study investigated patients who underwent CACS

10.3389/fcvm.2022.1053398

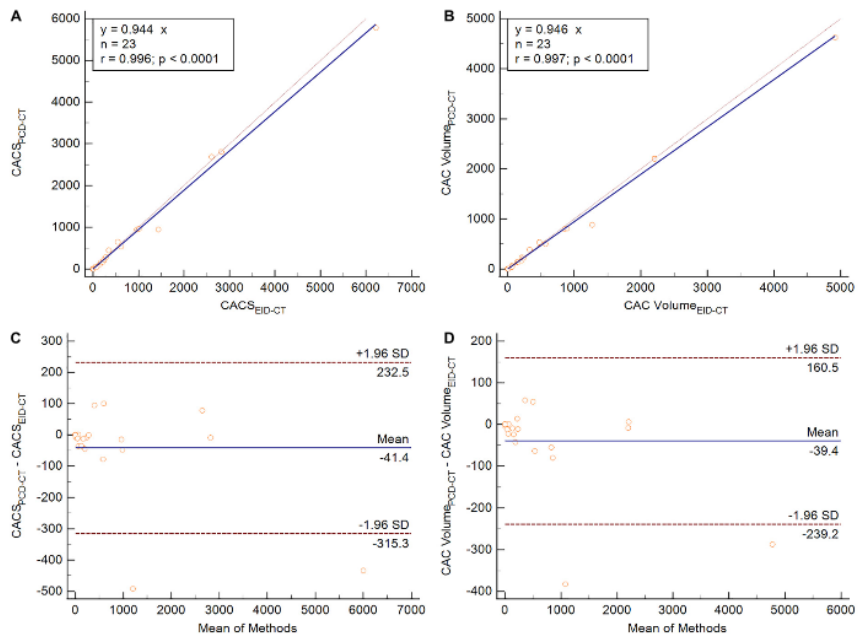

FIGURE 5
Patient study comparing CACS **(A,C)** and CAC volume **(B,D)** between PCD-CT and EID-CT in scatter- **(A,B)** and Bland-Altman plots **(C,D)**. SD, standard deviation; *r*, Spearmen correlation.

TABLE 3 Comparison of total and per-vessel values between EID-CT and PCD-CT in patients.

	EID-CT	PCD-CT	*p*	*r*	ICC	Bias	LoA
Total CACS	218.2 (18.5–876.4)	174.3 (11.1–872.7)	0.10	0.99	0.99	−41.4	−315.3/232.6
Total CAC volume	206.8 (15.9–782.6)	165.0 (9.8–731.6)	0.04	0.99	0.99	−37.6	−233.6/158.3
LM CACS	0.0 (0–21)	0.0 (0–26.9)	0.38	0.98	0.94	−5.6	−45.7/34.6
LM CAC volume	0.0 (0–19.1)	0.0 (0–19.1)	0.46	0.99	0.97	−3.0	−26.2/20.1
LAD CACS	91.0 (0.6–266.9)	96.3 (0.7–273.5)	0.22	0.99	0.99	16.1	−80.3/112.4
LAD CAC volume	78.0 (1.5–205.7)	83.1 (1.4–218.6)	0.35	0.99	0.99	8.2	−44.3/60.7
LCX CACS	53.1 (0–297.5)	16.7 (0–292.4)	0.11	0.97	0.95	−49.5	−356.1/257.0
LCX CAC volume	9.5 (0–47.3)	7.9 (0–45.4)	0.41	0.99	0.99	−0.2	−37.3/37.0
RCA CACS	53.1 (0–297.4)	16.7 (0–292.4)	0.30	0.97	0.95	−49.5	−356.1/257.0
RCA CAC volume	64.6 (0–291.7)	28.3 (0–277.2)	0.08	0.97	0.95	−41.2	−283.2/200.7

Values are median (interquartile range).
LM, left main, LAD, left anterior descending; LCX, left circumflex; RCA, right coronary artery; CACS, coronary artery calcium scoring; CAC, coronary artery calcium; ICC, intraclass correlation; LoA, limits of agreement.

on the EID-CT and simulated their virtual CACS risk class that would have been derived by the PCD-CT. According to our *in vitro* and *in vivo* evaluations, approximately 5% of patients would have been reclassified to a lower risk category with potential effects on clinical management such as initiation of optimal medical therapy. The new classification mostly affected patients who were classified immediately above the next category's cut off. One should thus be cautious on the risk of potential reclassification when measuring CACS on PCD-CT images. To compare CACS from PCD- to a dual-source EID-CT (of the same vendor), $CACS_{PCD-CT}$ may be multiplied by the factor of 1.056. Effects on prognostic and therapeutic implications and a potential change in risk stratification classes, however, have to be studied in future studies in larger cohorts.

Several attempts have been made to improve the conventional CACS protocol since its introduction. Recently, van Praagh et al. evaluated the optimization of several parameters in CACS for EID-CT systems from four different vendors compared to the standard CACS protocol (24). They reduced tube voltage to 100 kVp, radiation

TABLE 4 Reclassification study for simulated PCD-CT examinations.

	Original risk classification	New risk classification	Difference (%)
Agatston score category			
0	787	0	
1–10	62	5	8.06
11–100	132	5	3.79
101–400	144	10	6.94
>400	176	7	3.98
Total (>0)	514	27	5.25
Total	1,301		

Total number of patients (n).

dose to 75%, slice thickness to 1 or 1.25 mm and applied a higher iterative reconstruction level resulting in a 36 and 34% lower intra- and inter-scan variability and improved detection of small and low-density calcifications. However, these protocol modifications have not been applied to PCD-CT derived CACS yet.

There are some limitations to our study that need to be considered: First, the distribution of calcifications was imbalanced in the patient cohort. There were only a limited number of patients with severe calcification. Second, our patient cohort was limited to 23 patients and a larger study group would be desirable to improve the statistics of the model extended to the reclassification rates. Clinical implications such as new reclassification classes for PCD-CT based CACS have to be investigated in further studies. Third, PCD-CT scans were acquired at slightly lower radiation dose levels, thereby theoretically making them more prone to software detection errors as CACS depends on acquisition and reconstruction settings and the corresponding image noise levels. Low dose scans with high image noise may result in higher Agatston scores, because noise pixels exceeding the 130 HU threshold may be erroneously counted as calcifications. In addition, the in this study used lowest setting of iterative reconstruction (QIR off) may not the optimal reconstruction setting for PCD-CT based CACS. However, $CACS_{PCD-CT}$ systematically demonstrated lower CACS values in this study. Fourth, a ground truth for CACS was available only for phantom measurements. Differences and reclassification of *in vivo* data can therefore be interpreted only in relation to the phantom experiments, and we are unable to demonstrate which *in vivo* CACS measurement is more accurate. Fifth, differences in heart rate, radiation dose and other acquisition parameters including breath-hold and positioning could have affected the results. However, the analysis demonstrated systemic relationships that are unlikely caused by individual factors. Finally, we considered just one available phantom size, therefore, our results may not be applicable to different body types.

In conclusion, PCD-CT measures lower CACS values in both phantom and patient studies, resulting in reclassification of approximately 5% of individuals into lower risk groups. Compared to EID-CT, PCD-CT may be more accurate for physical quantification of calcifications. Further studies have to be conducted to evaluate optimized CACS PCD-CT imaging protocols and their potential effect on risk stratification and medical treatment.

Data availability statement

The raw data supporting the conclusions of this article will be made available by the authors, without undue reservation.

Ethics statement

The studies involving human participants were reviewed and approved by Institutional Review Board, Medical University of South Carolina, Charleston, SC, United States. The patients/participants provided their written informed consent to participate in this study.

Author contributions

EVW, MCH, and TE designed the study, interpreted the study data, and drafted the manuscript. PS, IMK, GJA, and DB acquired the data and substantially revised the manuscript. EZ, NF, JPG, and MMH performed the data analysis, supported the statistical analysis, and substantially revised the manuscript. JO'D and MJW advised the data reconstruction, supervised the data analysis, and edited/revised the manuscript. AV-S and UJS supervised the study conception and data interpretation and substantially edited the manuscript. All authors read and approved the final manuscript.

Funding

This work was supported by a research grant from Siemens Healthineers. The MAInz-DOC Doctoral College and the Kaltenbach Doctoral Scholarship of the German Heart Foundation supported EVW.

Conflict of interest

UJS received institutional research support and/or personal fees from Bayer, Bracco, Elucid Bioimaging, Guerbet, HeartFlow, Keya Medical, and Siemens. AV-S received institutional research support and/or personal fees from Elucid Bioimaging and Siemens. MJW was a stockholder, co-founder, and employee at Segmed and receives a personal research grant from the American Heart Association. TE received a speaker fee and travel support from Siemens Medical Solutions USA, Inc. JO'D was an employee of Siemens Medical Solutions USA, Inc.

The remaining authors declare that the research was conducted in the absence of any commercial or financial relationships that could be construed as a potential conflict of interest.

Publisher's note

References

1. Divakaran S, Cheezum M, Hulten E, Bittencourt M, Silverman M, Nasir K, et al. Use of cardiac CT and calcium scoring for detecting coronary plaque: implications on prognosis and patient management. *Br J Radiol.* (2015) 88:20140594. doi: 10.1259/bjr.20140594

2. Greenland P, Alpert J, Beller G, Benjamin E, Budoff M, Fayad Z, et al. 2010 ACCF/AHA guideline for assessment of cardiovascular risk in asymptomatic adults: executive summary: a report of the American college of cardiology foundation/American heart association task force on practice guidelines. *Circulation.* (2010) 122:2748–64. doi: 10.1161/CIR.0b013e3182051bab

3. Goff D Jr, Lloyd-Jones D, Bennett G, Coady S, D'Agostino R, Gibbons R, et al. 2013 ACC/AHA guideline on the assessment of cardiovascular risk: a report of the American college of cardiology/American heart association task force on practice guidelines. *Circulation.* (2014) 129(25 Suppl. 2):S49–73. doi: 10.1161/01.cir.0000437741.48606.98

4. Willemink M, Persson M, Pourmorteza A, Pelc N, Fleischmann D. Photon-counting CT: technical principles and clinical prospects. *Radiology.* (2018) 289:293–312. doi: 10.1148/radiol.2018172656

5. Eberhard M, Mergen V, Higashigaito K, Allmendinger T, Manka R, Flohr T, et al. Coronary calcium scoring with first generation dual-source photon-counting CT-first evidence from phantom and in-vivo scans. *Diagnostics.* (2021) 11:1703. doi: 10.3390/diagnostics11091708

6. van der Werf N, Si-Mohamed S, Rodesch P, van Hamersvelt R, Greuter M, Boccalini S, et al. Coronary calcium scoring potential of large field-of-view spectral photon-counting CT: a phantom study. *Eur Radiol.* (2022) 32:152–62. doi: 10.1007/s00330-021-08152-w

7. Groen J, Greuter M, Vliegenthart R, Suess C, Schmidt B, Zijlstra F, et al. Calcium scoring using 64-slice MDCT, dual source CT and EBT: a comparative phantom study. *Int J Cardiovasc Imaging.* (2008) 24:547–56. doi: 10.1007/s10554-007-9282-0

8. Agatston A, Janowitz W, Hildner F, Zusmer N, Viamonte M Jr, Detrano R. Quantification of coronary artery calcium using ultrafast computed tomography. *J Am Coll Cardiol.* (1990) 15:827–32. doi: 10.1016/0735-1097(90)90282-T

9. Obisesan O, Osei A, Uddin S, Dzaye O, Blaha M. An update on coronary artery calcium interpretation at chest and cardiac CT. *Radiol Cardiothorac Imaging.* (2021) 3:e200484. doi: 10.1148/ryct.2021200484

10. Willemink M, Vliegenthart R, Takx R, Leiner T, Budde R, Bleys R, et al. Coronary artery calcification scoring with state-of-the-art CT scanners from different vendors has substantial effect on risk classification. *Radiology.* (2014) 273:695–702. doi: 10.1148/radiol.14140066

11. Koo T, Li MYA. Guideline of selecting and reporting intraclass correlation coefficients for reliability research. *J Chiropr Med.* (2016) 15:155–63. doi: 10.1016/j.jcm.2016.02.012

12. Oliver M, Samuel E, Morley P, Young G, Kapur P. Detection of coronary-artery calcification during life. *Lancet.* (1964) 1:891–5. doi: 10.1016/S0140-6736(64)91625-3

13. Sangiorgi G, Rumberger J, Severson A, Edwards W, Gregoire J, Fitzpatrick L, et al. Arterial calcification and not lumen stenosis is highly correlated with atherosclerotic plaque burden in humans: a histologic study of 723 coronary artery segments using nondecalcifying methodology. *J Am Coll Cardiol.* (1998) 31:126–33. doi: 10.1016/S0735-1097(97)00443-9

14. Budoff M, Diamond G, Raggi P, Arad Y, Guerci A, Callister T, et al. Continuous probabilistic prediction of angiographically significant coronary artery disease using electron beam tomography. *Circulation.* (2002) 105:1791–6.

15. Blaha M, Cainzos-Achirica M, Greenland P, McEvoy J, Blankstein R, Budoff M, et al. Role of coronary artery calcium score of zero and other negative risk markers for cardiovascular disease: the multi-ethnic study of atherosclerosis (MESA). *Circulation.* (2016) 133:849–58. doi: 10.1161/CIRCULATIONAHA.115.018524

16. Carr J, Jacobs D Jr, Terry J, Shay C, Sidney S, Liu K, et al. Association of coronary artery calcium in adults aged 32 to 46 years with incident coronary heart disease and death. *JAMA Cardiol.* (2017) 2:391–9. doi: 10.1001/jamacardio.2016.5493

17. Detrano R, Guerci A, Carr J, Bild D, Burke G, Folsom A, et al. Coronary calcium as a predictor of coronary events in four racial or ethnic groups. *N Engl J Med.* (2008) 358:1336–45. doi: 10.1056/NEJMoa072100

18. Hoffmann U, Ferencik M, Cury R, Pena A. Coronary CT angiography. *J Nucl Med.* (2006) 47:797–806.

19. Mergen, V, Higashigaito K, Allmendinger T, Manka R, Euler A, Alkadhi H, et al. Tube voltage-independent coronary calcium scoring on a first-generation dual-source photon-counting CT-a proof-of-principle phantom study. *Int J Cardiovasc Imaging.* (2022) 38:905–12. doi: 10.1007/s10554-021-02466-y

20. van der Werf N, van Gent M, Booij R, Bos D, van der Lugt A, Budde R, et al. Dose reduction in coronary artery calcium scoring using mono-energetic images from reduced tube voltage dual-source photon-counting CT data: a dynamic phantom study. *Diagnostics.* (2021) 11:2192. doi: 10.3390/diagnostics11122192

21. Emrich T, Aquino G, Schoepf U, Braun F, Risch F, Bette S, et al. Coronary computed tomography angiography-based calcium scoring: in vitro and in vivo validation of a novel virtual noniodine reconstruction algorithm on a clinical, first-generation dual-source photon counting-detector system. *Invest Radiol.* (2022) 57:536–43. doi: 10.1097/RLI.0000000000000868

22. Willemink M, van der Werf N, Nieman K, Greuter M, Koweek L, Fleischmann D. Coronary artery calcium: a technical argument for a new scoring method. *J Cardiovasc Comput Tomogr.* (2019) 13:347–52. doi: 10.1016/j.jcct.2018.10.014

23. Budoff M, Kessler P, Gao Y, Qunibi W, Moustafa M, Mao S. The interscan variation of CT coronary artery calcification score: analysis of the calcium acetate renagel comparison (CARE)-2 study. *Acad Radiol.* (2008) 15:58–61. doi: 10.1016/j.acra.2007.08.011

24. van Praagh G, Wang J, van der Werf N, Greuter M, Mastrodicasa D, Nieman K, et al. Coronary artery calcium scoring: toward a new standard. *Invest Radiol.* (2022) 57:13–22. doi: 10.1097/RLI.0000000000000808

2.2 „Intra-individual comparison of coronary artery stenosis measurements between energy-integrating detector CT and photon-counting detector CT”

Dieses Kapitel basiert auf der bereits veröffentlichten Open-Access-Publikation:

Wolf EV, Gnasso C, Schoepf UJ, Halfmann MC, O'Doherty J, Zsarnoczay E, Varga-Szemes A, Emrich T, Fink N. Intra-individual comparison of coronary artery stenosis measurements between energy-integrating detector CT and photon-counting detector CT. Imaging, 2023 Dec 15(2), 61-68. doi: 10.1556/1647.2023.00156.

AKADÉMIAI KIADÓ

IMAGING

ORIGINAL ARTICLE

Intra-individual comparison of coronary artery stenosis measurements between energy-integrating detector CT and photon-counting detector CT

ELIAS V. WOLF[1,2†], CHIARA GNASSO[1,3†], U. JOSEPH SCHOEPF[1], MORITZ C. HALFMANN[2], JIM O'DOHERTY[1,4], EMESE ZSARNOCZAY[1,5], AKOS VARGA-SZEMES[1], TILMAN EMRICH[1,2*] and NICOLA FINK[1,6]

[1] Department of Radiology and Radiological Science, Division of Cardiovascular Imaging, Medical University of South Carolina, Charleston, SC, USA

[2] Department of Diagnostic and Interventional Radiology, University Medical Center of the Johannes Gutenberg-University Mainz, Mainz, Germany

[3] Clinical and Experimental Radiology Unit, Experimental Imaging Center, IRCCS San Raffaele Scientific Institute, Milan, Italy

[4] Siemens Medical Solutions, 40 Liberty Boulevard, Malvern, PA, USA

[5] Medical Imaging Center, Semmelweis University, Budapest, Hungary

[6] Department of Radiology, University Hospital, LMU Munich, Munich, Germany

Received: May 31, 2023 • Revised manuscript received: June 30, 2023 • Accepted: July 6, 2023

ABSTRACT

Purpose: To compare intra-individual percentage diameter stenosis (PDS) measurements of coronary artery stenoses between energy-integrating detector computed tomography (EID-CT) and a clinical photon-counting detector computed tomography (PCD-CT) systems using similar acquisition and reconstruction settings.

Methods: Patients (n = 23, mean age of 65 ± 12.1 years, out of these 16 (69.6%) male) were imaged on a conventional EID- and a clinical PCD-CT system with a median of 5.5 (3.0–12.5) days apart. Sequential CCTA scans were acquired and reconstructed using similar settings, including a vascular Bv36 kernel, a tube voltage of 110 kVp for EID-CT vs 120 kVp for PCD-CT, a slice thickness of 0.5 for EID-CT vs 0.6 for PCD-CT, and an iterative reconstruction strength of 3 on EID-CT vs a virtual monoenergetic reconstruction at 55 keV and quantum iterative reconstruction level of 3 on PCD-CT. Radiation dose, contrast volume, and injection parameters were matched as similarly as possible between the systems. PDS measurements were performed according to the coronary artery disease reporting and data system (CAD-RADS) by two trained readers and compared between the different modalities using the Wilcoxon rank sum test, Spearman correlation, and Bland-Altman analysis.

Results: PCD-CT measured significantly lower PDS values than EID-CT [PDS_{EID-CT}: 45.1% (35.1%–64.0%) vs. PDS_{PCD-CT} 44.2% (32.4%–61.0%), $P < 0.0001$]. This difference led to a mean bias of 1.8 (LoA −3.0/6.5) with an excellent ICC (0.99) value among EID- and PCD-CT. The mean intra-individual deviation between the examinations was 1.8% between the scanners. This led to CAD-RADS re-classification in 3/23 cases (13.0%, new-lower class) for the first reader, and in 4/23 cases (13.0%, new-lower and 4.4%, new-higher class) for the second reader. Inter-reader agreement between the two readers for each stenosis was very strong (ICC = 0.98).

Conclusions: Coronary artery stenosis measurements from PCD-CT correlate strongly to EID-CT-based measurements, despite the tendency of the measurement from PCD-CT being lower. This difference led to a change in CAD-RADS classification in 17.4% of patients. The effects on clinical decision-making, downstream testing, and prognosis have to be evaluated in future studies.

KEYWORDS

stenosis, coronary artery disease, photon-counting detector computed tomography, energy-integrating detector computed tomography

IMAGING 15 (2023) 2, 61–68
DOI: 10.1556/1647.2023.00156

†EVW and CG contributed equally to this publication.

*Corresponding author.
Tel.: +49 6131177358.
E-mail: Tilman.Emrich@unimedizin-mainz.de

AKJournals

Introduction

Coronary artery disease (CAD) is the leading cause of death worldwide [1]. Over the last two decades, coronary CT angiography (CCTA) has emerged as one of the most commonly used modalities for the clinical evaluation of stable CAD [2, 3]. Accurate CT-based quantification of coronary artery stenosis is critical because stenosis severity in combination with calcium scoring guides clinical decision-making [4]. In this context, CCTA has already been shown to have excellent negative predictive value and moderate positive predictive value for the detection and evaluation of CAD, especially in patients with low or intermediate risk [5, 6]. However, the positive predictive value of CCTA suffers as the burden of calcium in the coronary arteries increases due to calcium blooming artifacts [7].

Recently, photon-counting detector computed tomography (PCD-CT) has become clinically available, enabling direct conversion of x-ray photon radiation into an electrical signal instead of using an intermediate conversion into visible light photons through a scintillator [8]. Compared with conventional energy integrating detector CT (EID-CT), PCD-CT offers several distinct advantages, including higher spatial resolution, lower image noise, and constantly available spectral image information [9–16]. These advantages have the potential to allow for more accurate stenosis quantification and overcome previous limitations in CT-based cardiac imaging. However, due to the novelty of this technique, analyses comparing intra-individual measurements from PCD- and EID-CT using similar settings are required to ensure transferability into clinical practice.

We hypothesized that percentage diameter stenosis (PDS) measurements with PCD-CT yield similar results compared to the conventional, clinical-standard EID-CT when acquired and reconstructed similarly. Thus, this study aims to intra-individually compare PDS measurements between a first-generation dual-source PCD-CT and a state-of-the-art conventional dual-source EID-CT.

Materials & methods

Patients

The protocol of this single-center, Health Insurance Portability and Accountability Act-compliant, study was approved by the local Institutional Review Board (IRB). Patients were prospectively enrolled based on the following inclusion criteria: (1) clinical indication for cardiac imaging; and (2) >18 years of age. The following exclusion criteria were applied: (1) contraindication to iodine-based contrast media; (2) reduced kidney function (glomerular filtration rate <45 mL min^{-1} m^{-2}); (3) pregnancy or lactation, and (4) unable to be consented. All patients provided written informed consent and underwent an electrocardiogram (ECG)-gated CCTA examinations on both CT systems between August 2021 and March 2022.

Data acquisition and image reconstruction

Both the conventional EID-CT (SOMATOM Force, Siemens Healthineers, Erlangen, Germany) and a first-generation, clinical PCD-CT (NAEOTOM Alpha, Siemens) were used to perform CCTA examinations. The PCD-CT is equipped with two photon-counting cadmium telluride (CdTe) detectors, each with a collimation of 144 × 0.4 mm, which enables spectral CT data acquisition at a high temporal resolution. The tube voltage was set to 110 kVp for the EID-CT, which was the standard protocol used at our institution, while it was set to 120 kVp for the PCD-CT per vendor recommendations.

A sequential cardiac protocol was used for all scans, which included ECG triggering and a triphasic contrast injection protocol and a constant injection rate for all three phases (4 mL s^{-1}). This involved injecting an initial bolus of nonionic iodinated contrast agent (50 mL, iopromide 370 mgI mL^{-1}, Ultravist, Bayer Healthcare), followed by a 50% mixture of contrast agent and saline solution (20 mL), and a saline chaser (25 mL). If it was not clinically contraindicated, patients were given 0.4 mg nitroglycerin about 5 min before the scan, and those with heart rates above 70 beats per minute received 5 mg metoprolol intravenously.

CT images were directly reconstructed on the scanners. All reconstructions were performed in the phase with the least motion artifacts (best diastolic or systolic phase), using a body vascular kernel (Bv36) a slice thickness of 0.5 and 0.6 mm for the EID-CT and the PCD-CT, respectively. Iterative reconstruction algorithms were applied at strength level 3 for both scanners, using advanced modeled iterative reconstruction (ADMIRE) for the EID-CT and quantum iterative reconstructions (QIR) for the PCD-CT. Detailed acquisition and reconstruction parameters for both scanners can be found in Table 1.

Stenosis measurements

Measurements were performed by two readers with 2 and 4 years of experience in cardiovascular radiology and under the supervision of a board-certified cardiovascular radiologist with 12 years of experience. The supervisor selected relevant stenoses with at least 20% of vessel obstruction. Both readers independently assessed each stenosis in a blinded fashion.

Table 1. CT acquisitions and reconstructions

Modality	EID-CT	PCD-CT
Tube potential (kVp)	110	120
Monoenergetic level (keV)	n/a	55
Iterative reconstruction	Admire 3	QIR 3
Reconstruction kernel	Bv36	Bv36
Slice thickness (mm)	0.5	0.6
Field of View (mm)	200	200
Matrix size	512 × 512	512 × 512

QIR, quantum iterative reconstruction; EID-CT, energy-integrating computed tomography; PCD-CT, photon-counting detector computed tomography.

Stenosis measurements were based on a semi-automated segmentation of the remaining coronary artery lumen using a commercially available software solution (CT Coronary, syngo.via Version VB60, Siemens). An example case illustrating the visualization for stenosis measurements is shown in Fig. 1. Quantitative analysis of the stenoses was conducted on cross-sectional images and according to established methods using the diameter proximal and distal to the stenosis as reference [17]. The reference diameters were measured in a plaque-free portion of the same vessel as close as possible to the selected stenosis.

Based on these measurements, the PDS was calculated with a validated formula as described previously [18]:

$$PDS = 1 - \frac{D_S}{D_V}$$

in which D_S is the minimal remaining vessel lumen of the coronary artery stenosis and D_V represents the average reference diameter proximal and distal to the stenosis.

For reliable results, window-level settings were kept constant (C450 HU/W1500 HU) in the PCD- and EID-CT measurements. The readers also classified the plaques as being either calcified or mixed.

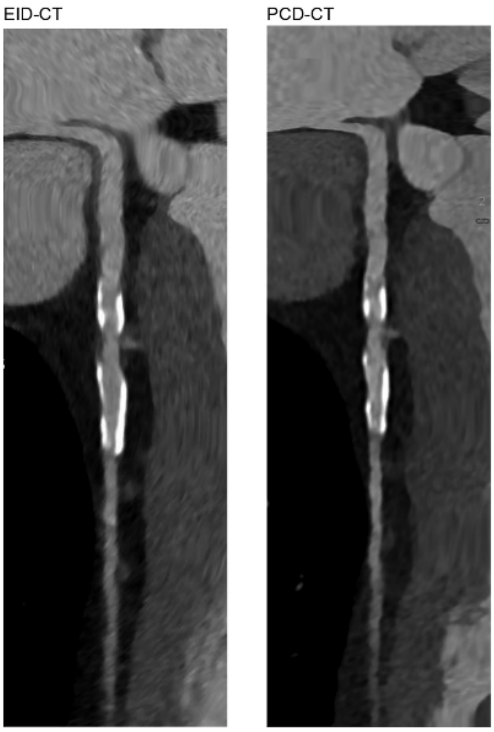

Fig. 1. Representative image in a patient scanned with the EID- and PCD-CT

Furthermore, patients were assessed according to the Coronary Artery Disease Reporting and Data System (CAD-RADS) depending on the measured PDS as follows: CAD-RADS 0 – 0%; CAD-RADS 1 – 1-24%; CAD-RADS 2 – 25-49%; CAD-RADS 3 – 50-74%; CAD-RADS 4 – 75-99%; CAD-RADS 4 – 100% [19].

Statistical analysis

Dedicated software (SPSS Statistics for Windows, Version 21.0, IBM Corp Armonk, NY; MedCalc for Windows, version 15.0, MedCalc Software, Ostend, Belgium; GraphPad Prism, Version 9 for macOS, San Diego, CA, USA) was used for statistical analysis. The data was tested for normality using the Kolmogorov-Smirnov test. For normally distributed data, mean ± standard deviation (SD) was used, while median with interquartile range was used for non-normally distributed data. Categorical variables were reported as frequencies and proportions. The means' distribution was compared with independent samples *t*-test for normally-distributed variables or Mann-Whitney *U* test for non-parametric variables. The difference between the two CT stenosis measurements was compared using the Wilcoxon rank sum test, and a *p*-value of 0.05 was deemed significant. The mean bias and the upper and lower limits of agreement (LoA) between the two approaches were evaluated using Bland-Altman analysis. The correlation between PDS values from EID- and PCD-CT was measured using the Spearman correlation coefficient (r). The agreements between the two CT systems and the two readers were measured using intraclass correlation coefficients (ICC), with the following interpretations: 0.0 to 0.3, lack of agreement; 0.31 to 0.5, weak agreement; 0.51 to 0.7, moderate agreement; 0.71 to 0.9, strong agreement; and 0.91 to 1.00, very strong agreement [20].

Results

The study included 23 patients (16 men) with a mean age of 65 ± 12.1 years and a total of 42 evaluated stenoses, comprised of 31 (73.8%) mixed and 11 (26.2%) calcified plaques. The PCD-CT scan was conducted a median of 5.5 (3.0–12.5) days after the EID-CT scan. The median radiation dose for scans obtained with PCD-CT was significantly lower compared to those performed with EID-CT [CTDIvol EID-CT: 38.3 (20.9–58.0) mGy vs PCD-CT: 28.0 (18.2–54.2) mGy, $P < 0.05$]. Clinical CT examinations included the following indications: 13 (56.5%) stable chest pain/CAD, 7 (30.4%) valvular disease, 3 (13.0%) structural heart disease. A detailed listing of the study population, scan conditions, and plaque characterization is given in Table 2.

Stenosis evaluation

Overall, the $PDS_{PCD\text{-}CT}$ measurements were significantly lower than corresponding $PDS_{EID\text{-}CT}$ values ($PDS_{EID\text{-}CT}$: 45.1% (35.1%–64.0%) vs. $PDS_{PCD\text{-}CT}$: 44.2% (32.4%–61.0%), $P < 0.0001$, mean bias 1.8, LoA −3.0/6.5). Nevertheless,

Table 2. Patient characteristics

n	23	
Female (%)	7 (30.4)	
Age (years)	65 ± 12.1	
BMI (kg m^{-2})	30.1 ± 7.1	
Time between scans (days)	5.5 (3.0–12.5)	
	EID-CT	**PCD-CT**
Heart rate (bpm)	64.1 ± 11.0, *	65.3 ± 10.8, *
$CTDI_{vol}$ (mGy)	38.3 (20.9–58.0), **	28.0 (18.2–54.2), **
DLP (mGy*cm)	647.8 (339.4–1055.1), ***	557.5 ± 384.7, ***
Mixed Plaques	31 (73.8%)	
Calcified Plaques	11 (26.2%)	

*$P = 0.4713$.
**$P = 0.0116$.
***$P = 0.0046$.
Values are mean ± standard deviation, median (interquartile range), *n* (frequencies).
BMI, body mass index; CTDI, computer tomography dose index; DLP, dose length product; EID-CT, energy-integrating computed tomography; PCD-CT, photon-counting detector computed tomography.

PDS_{PCD-CT} showed very strong correlation and agreement with PDS_{EID-CT} ($r = 0.988$, ICC = 0.99). The mean measurement deviation between individual stenoses amounted to a 1.8% difference between the scanners. Figure 2 demonstrates the correlation between PDS values from EID- and PCD-CT. Figure 3 displays the differences between the individual measurements from the EID- and PCD-CT.

Reclassification of CAD-RADS categories

Based on the degree of stenosis, patients were assigned a CAD-RADS score. Compared to the initial classification based on the EID-CT scan, measurements derived from PCD-CT scans led to a new-lower classification in three patients (3/23 cases, 13.0%) for both readers and to a new-higher classification in one patient (1/23 cases, 4.4%) for reader 2. This led to a per-patient CAD-RADS re-classification in 17.4% of cases. Details of the per-patient and per-vessel CAD-RADS category re-classifications are provided in Fig. 4, Table 3 and Supplementary Table S1. Agreement between the readers was very strong for stenosis measurements (ICC = 0.97) between the two CT systems.

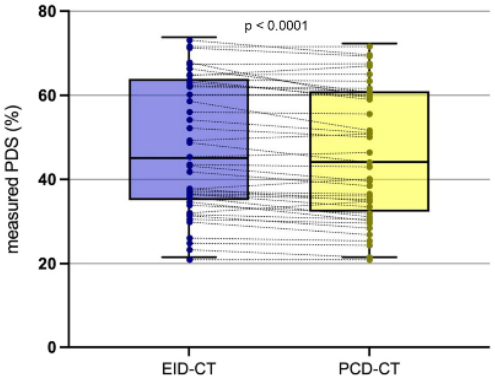

Fig. 3. Box plot with line diagram shows the comparison of percent diameter stenosis (PDS) values between EID-CT and PCD-CT with a *p*-value from a paired Wilcoxon test

Discussion

This prospective study investigated coronary artery stenosis measurements between EID- and PCD-CT in an intra-individual patient setting. Major findings were: 1) PCD-CT PDS values measured lower on average compared to the measurements on EID-CT. 2) This led to CAD-RADS re-classification in approximately 17% of patients. 3) Despite the instances of re-classification, there was still a very strong

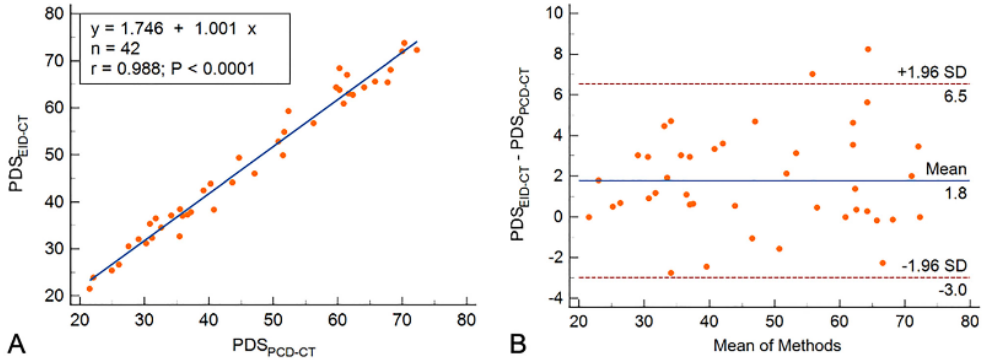

Fig. 2. Scatterplot (A) and Bland-Altman plot (B) show the correlation of percent diameter stenosis (PDS) between EID-CT and PCD-CT

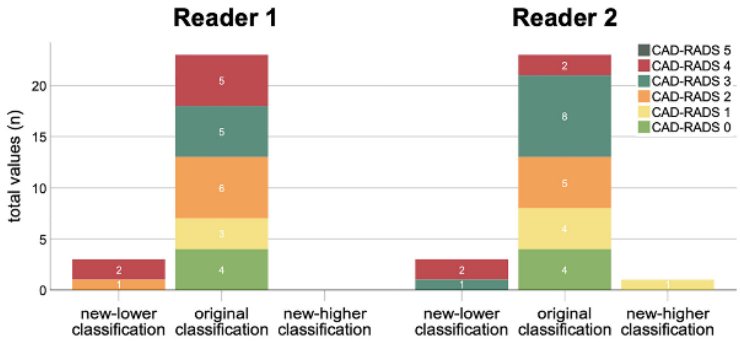

Fig. 4. Bar diagram show the original and re-classification of CAD-RADS categories for reader 1 and 2

Table 3. Re-classification of CAD-RADS categories

Per-Patient Classification						
	Reader 1			Reader 2		
CAD-RADS Score Category	New-lower risk classification	Original classification	New-higher risk classification	New-lower risk classification	Original classification	New-higher risk classification
0		4			4	
1		3			4	1
2	1	6			5	
3		5		1	8	
4	2	5		2	2	
5		0			0	
Total	**3**	**23**		**3**	**23**	**1**
Difference (%)	13.0			13.0		4.4

correlation and agreement of coronary stenosis measurements between the two CT systems.

CCTA is considered a first-line test in the evaluation of CAD due to its high sensitivity and negative predictive value in patients with low and intermediate risk of CAD [5, 6]. Additionally, CCTA enables the evaluation of coronary stenosis and plaque composition, providing valuable information for prognostic stratification [21, 22]. However, CCTA is restricted by a moderate positive predictive value due to artifacts that can lead to overestimation of stenoses, particularly from high-density calcifications or stents [23–25]. For high-density calcifications, errant stenosis measurements are induced by calcium blooming artifacts, which occur more frequently as calcium density increases [26]. The inappropriate stenosis measurements are caused by different tissue attenuations within the same imaged voxel [27]. Inaccurate PDS measurements with a stenosis overestimation can lead to unnecessary ICA [25, 26].

It has been demonstrated that PCD-CT reduces calcium blooming through increased spatial resolution and better decomposition of materials [28]. Despite similar reconstructions in our study between the PCD- and EID-CT systems, PCD-CT seemed to be less prone to calcium blooming and therefore resulted in lower PDS value measurements. However, the overestimation of PDS by standard resolution CCTA has been investigated by several phantom studies using EID- and PCD-CT [18, 29, 30]. Based on these prior publications, it can be implied that the PCD-CT *in-vivo* measurements in our study are more accurate than the EID-CT measurements, which is currently one of the state-of-the-art CT systems in clinical settings.

The lower PDS measurements would follow with a new-lower risk classification in patients and therefore has an impact on the CAD-RADS system. We demonstrated a new per-patient CAD-RADS classification in approximately 17% of our patients. Similarly, a previous study compared the intra-individual coronary artery calcium score using identical scan parameters between EID- and PCD-CT [12]. The study revealed a new-lower reclassification rate for the PCD-CT of approximately 5% compared to the EID-CT, which suggests a role in evaluating the plaque burden in patients. An accurate CT-based quantification of stenosis degrees is of great importance and represents the basis for the risk assessment of CAD, which guides clinical management [31]. However, most patients still received the same CAD-RADS category with the PCD-CT acquisition compared to the EID-CT, and there was a high degree of agreement between stenosis grading and CAD-RADS classification from both CT systems. On the other hand, through further improvements such as of the spatial resolution on the PCD-CT, it might have the potential

to improve the positive predictive value of CCTA and thereby reduce unnecessary downstream testing in patients.

Despite the advantages demonstrated in this study using similar reconstructions between EID- and PCD-CT, PCD-CT systems offer various other advantages. For example, a new image reconstruction algorithm (PureLumen, Siemens) could improve stenosis assessment on the PCD-CT through removing calcified plaques and displaying the contrasted vessel [18]. Allmendinger et al. explored this concept in a phantom study that demonstrated better agreement of stenosis grading using PureLumen than a standard virtual monoenergetic reconstruction on PCD-CT. Furthermore, an ultra-high resolution (UHR) mode of the PCD-CT can be employed to reduce calcium blooming, leading to a higher image quality of calcified coronary arteries [32]. Koons et al. performed a study comparing stenosis measurements on a PCD- and EID-CT of a stationary phantom and showed more accurate measurements using UHR vs standard resolution (SR) [29]. They demonstrated better performance of the UHR in detecting the severity of differently arranged stenoses. These results were confirmed and expanded by Zsarnoczay et al. who demonstrated that the use of UHR led to more accurate PDS measurements in a motion phantom compared to SR acquisition over a range of different heart rates [30]. Generally, there was an overestimation of stenoses found in the phantom for both UHR and SR, but the UHR measurements were closer to the true values. In addition, these new approaches allow the reduction of calcium blooming artifacts to improve spatial resolution of the PCD-CT. However, *in-vivo* validation in prospective cohorts is currently lacking and is the subject of ongoing research protocols.

There are some limitations to our study: First, there were only 23 patients included, and a larger study group would be desirable. However, larger study cohorts with repeated CT scans performed within a short time range are rare. Second, our *in-vivo* study population consisted of an unequal distribution of calcifications. On the other hand, the distribution of the CAD-RADS classes was balanced over the patient population in this study. Third, differences in slice thickness/increment and the tube potential could have affected the results. Differences in radiation doses were due to ethical regulations requiring a lower or similar dose level for the PCD-CT. It would be expected that a lower radiation dose would worsen the image quality of PCD-CT images and potentially worsen stenosis measurements, but our results demonstrated improved PDS reading on the PCD-CT despite the lower radiation doses compared to the EID-CT images. Finally, it should be noted that this investigation lacks an invasive correlation, which is typically regarded as a ground truth, and thus warrants further investigation in clinical studies.

Conclusion

In conclusion, PDS measurements on PCD-CT are highly correlated but generally lower compared to the measurements from EID-CT using similar reconstruction settings. The discrepancy in stenosis measurements between the two CT systems resulted in per-patient CAD-RADS re-classification in 17.4% of cases. Further studies are expected to evaluate optimized PCD-CT imaging protocols for PDS evaluation and to investigate its effects on the clinical decision-making process.

Authors' contribution: EVW, CG, MCH and TE designed the study, interpreted the study data and drafted the manuscript. NF and EZ performed data analysis, supported statistical analysis, and substantially revised the manuscript. JOD advised data reconstruction, supervised data analysis and edited/revised the manuscript. AV-S and UJS supervised the study conception and data interpretation and substantially edited the manuscript. All authors read and approved the final manuscript.

Conflict of interest: UJS received institutional research support and/or personal fees from Bayer, Bracco, Elucid Bioimaging, Guerbet, HeartFlow, Keya Medical, and Siemens. AV-S received institutional research support and/or personal fees from Elucid Bioimaging and Siemens. TE received a speaker fee, travel and institutional research support from Siemens Medical Solutions USA, Inc. JO'D is an employee of Siemens Medical Solutions USA, Inc.

Funding sources: This work was supported by a research grant from Siemens Healthineers. The MAInz-DOC Doctoral College and the Kaltenbach Doctoral Scholarship of the German Heart Foundation supported EVW.

Ethical statement: The studies involving human participants were reviewed and approved by Institutional Review Board, Medical University of South Carolina, SC, United States. The patients/participants provided their written informed consent to participate in this study.

Supplementary data

Supplementary data to this article can be found online at https://doi.org/10.1556/1647.2023.00156.

REFERENCES

[1] Malakar AK, Choudhury D, Halder B, Paul P, Uddin A, Chakraborty S: A review on coronary artery disease, its risk factors, and therapeutics. J Cell Physiol 2019; 234(10): 16812–23.

[2] Knuuti J, Wijns W, Saraste A, Capodanno D, Barbato E, Funck-Brentano C, et al.: 2019 ESC Guidelines for the diagnosis and management of chronic coronary syndromes. Eur Heart J 2020; 41(3): 407–77.

[3] Moss AJ, Williams MC, Newby DE, Nicol ED: The updated NICE guidelines: cardiac CT as the first-line test for coronary artery disease. Curr Cardiovasc Imaging Rep 2017; 10(5): 15.

[4] Cury RC, Abbara S, Achenbach S, Agatston A, Berman DS, Budoff MJ, et al.: CAD-RADS(TM) coronary artery disease – reporting and data system. An expert consensus document of the

Society of Cardiovascular Computed Tomography (SCCT), the American College of Radiology (ACR) and the North American Society for Cardiovascular Imaging (NASCI). Endorsed by the American College of Cardiology. J Cardiovasc Comput Tomogr 2016; 10(4): 269–81.

[5] Knuuti J, Ballo H, Juarez-Orozco LE, Saraste A, Kolh P, Rutjes AWS, et al.: The performance of non-invasive tests to rule-in and rule-out significant coronary artery stenosis in patients with stable angina: A meta-analysis focused on post-test disease probability. Eur Heart J 2018; 39(35): 3322–30.

[6] Haase R, Schlattmann P, Gueret P, Andreini D, Pontone G, Alkadhi H, et al.: Diagnosis of obstructive coronary artery disease using computed tomography angiography in patients with stable chest pain depending on clinical probability and in clinically important subgroups: meta-analysis of individual patient data. BMJ 2019; 365: l1945.

[7] Chao SP, Law WY, Kuo CJ, Hung HF, Cheng JJ, Lo HM, et al.: The diagnostic accuracy of 256-row computed tomographic angiography compared with invasive coronary angiography in patients with suspected coronary artery disease. Eur Heart J 2010; 31(15): 1916–23.

[8] Willemink MJ, Persson M, Pourmorteza A, Pelc NJ, Fleischmann D. Photon-counting CT: Technical principles and clinical prospects. Radiology 2018; 289(2): 293–312.

[9] Aquino GJ, O'Doherty J, Schoepf UJ, Ellison B, Byrne J, Fink N, et al.: Myocardial characterization with extracellular volume mapping with a first-generation photon-counting detector CT with MRI reference. Radiology 2023; 307(2):e222030.

[10] Emrich T, O'Doherty J, Schoepf UJ, Suranyi P, Aquino G, Kloeckner R, et al.: Reduced iodinated contrast media administration in coronary CT angiography on a clinical photon-counting detector CT system: a phantom study using a dynamic circulation model. Invest Radiol 2023; 58(2): 148–55.

[11] Graafen D, Emrich T, Halfmann MC, Mildenberger P, Duber C, Yang Y, et al.: Dose reduction and image quality in photon-counting detector high-resolution computed tomography of the chest: routine clinical data. J Thorac Imaging 2022; 37(5): 315–22.

[12] Wolf EV, Halfmann MC, Schoepf UJ, Zsarnoczay E, Fink N, Griffith JP, 3rd, et al.: Intra-individual comparison of coronary calcium scoring between photon counting detector- and energy integrating detector-CT: effects on risk reclassification. Front Cardiovasc Med 2022; 9: 1053398.

[13] Euler A, Higashigaito K, Mergen V, Sartoretti T, Zanini B, Schmidt B, et al.: High-pitch photon-counting detector computed tomography angiography of the aorta: intraindividual comparison to energy-integrating detector computed tomography at equal radiation dose. Invest Radiol 2022; 57(2): 115–21.

[14] Emrich T, Aquino G, Schoepf UJ, Braun FM, Risch F, Bette SJ, et al.: Coronary computed tomography angiography-based calcium scoring: in vitro and in vivo validation of a novel virtual noniodine reconstruction algorithm on a clinical, first-generation dual-source photon counting-detector system. Invest Radiol 2022; 57(8): 536–43.

[15] Fink N, Zsarnoczay E, Schoepf UJ, Griffith JP, 3rd, Wolf EV, O'Doherty J, et al.: Photon counting detector CT-based virtual noniodine reconstruction algorithm for in vitro and in vivo coronary artery calcium scoring: impact of virtual monoenergetic and quantum iterative reconstructions. Invest Radiol 2023. https://doi.org/10.1097/RLI.0000000000000959.

[16] Zsarnoczay E, Varga-Szemes A, Emrich T, Szilveszter B, van der Werf NR, Mastrodicasa D, et al.: Characterizing the heart and the myocardium with photon-counting CT. Invest Radiol 2023; 58(7): 505–14.

[17] Dewey M, Rutsch W, Schnapauff D, Teige F, Hamm B: Coronary artery stenosis quantification using multislice computed tomography. Invest Radiol 2007; 42(2): 78–84.

[18] Allmendinger T, Nowak T, Flohr T, Klotz E, Hagenauer J, Alkadhi H, et al.: Photon-counting detector CT-based vascular calcium removal algorithm: assessment using a cardiac motion phantom. Invest Radiol 2022; 57(6): 399–405.

[19] Cury RC, Leipsic J, Abbara S, Achenbach S, Berman D, Bittencourt M, et al.: CAD-RADS 2.0-2022 coronary artery disease – reporting and data system.: an expert consensus document of the Society of Cardiovascular Computed Tomography (SCCT), the American College of Cardiology (ACC), the American College of Radiology (ACR) and the North America Society of Cardiovascular Imaging (NASCI). J Am Coll Radiol 2022; 19(11): 1185–212.

[20] Koo TK, Li MY: A guideline of selecting and reporting intraclass correlation coefficients for reliability research. J Chiropr Med 2016; 15(2): 155–63.

[21] Mergen V, Eberhard M, Manka R, Euler A, Alkadhi H: First in-human quantitative plaque characterization with ultra-high resolution coronary photon-counting CT angiography. Front Cardiovasc Med 2022; 9: 981012.

[22] Gulati M, Levy PD, Mukherjee D, Amsterdam E, Bhatt DL, Birtcher KK, et al.: 2021 AHA/ACC/ASE/CHEST/SAEM/SCCT/SCMR guideline for the evaluation and diagnosis of chest pain: a report of the American College of Cardiology/American Heart Association Joint Committee on Clinical Practice Guidelines. Circulation 2021; 144(22): e368–454.

[23] Renker M, Nance JW, Jr., Schoepf UJ, O'Brien TX, Zwerner PL, Meyer M, et al.: Evaluation of heavily calcified vessels with coronary CT angiography: comparison of iterative and filtered back projection image reconstruction. Radiology 2011; 260(2): 390–9.

[24] Zhang S, Levin DC, Halpern EJ, Fischman D, Savage M, Walinsky P: Accuracy of MDCT in assessing the degree of stenosis caused by calcified coronary artery plaques. AJR Am J Roentgenol 2008; 191(6): 1676–83.

[25] Song YB, Arbab-Zadeh A, Matheson MB, Ostovaneh MR, Vavere AL, Dewey M, et al.: Contemporary discrepancies of stenosis assessment by computed tomography and invasive coronary angiography. Circ Cardiovasc Imaging 2019; 12(2): e007720.

[26] Vavere AL, Arbab-Zadeh A, Rochitte CE, Dewey M, Niinuma H, Gottlieb I, et al.: Coronary artery stenoses: Accuracy of 64-detector row CT angiography in segments with mild, moderate, or severe calcification–a subanalysis of the CORE-64 trial. Radiology 2011; 261(1): 100–8.

[27] Kalisz K, Buethe J, Saboo SS, Abbara S, Halliburton S, Rajiah P: Artifacts at cardiac CT: physics and solutions. Radiographics 2016; 36(7): 2064–83.

[28] Symons R, De Bruecker Y, Roosen J, Van Camp L, Cork TE, Kappler S, et al.: Quarter-millimeter spectral coronary stent imaging with photon-counting CT: initial experience. J Cardiovasc Comput Tomogr 2018; 12(6): 509–15.

[29] Koons E, VanMeter P, Rajendran K, Yu L, McCollough C, Leng S: Improved quantification of coronary artery luminal stenosis in the

presence of heavy calcifications using photon-counting detector CT. Proc SPIE Int Soc Opt Eng 2022; 12031.

[30] Zsarnoczay E, Fink N, Schoepf UJ, O'Doherty J, Allmendinger T, Hagenauer J, et al.: Ultra-high resolution photon-counting coronary CT angiography improves coronary stenosis quantification over a wide range of heart rates – a dynamic phantom study. Eur J Radiol 2023; 161: 110746.

[31] Saraste A, Knuuti J: Evaluation of coronary artery disease after computed tomography angiography. Eur Heart J Cardiovasc Imaging 2018; 19(4): 378–9.

[32] Mergen V, Sartoretti T, Baer-Beck M, Schmidt B, Petersilka M, Wildberger J, et al.: Ultra-high-resolution coronary CT angiography with photon-counting detector CT: feasibility and image characterization. Invest Radiol 2022; 57(12): 780–8.

2.3 „Photon-Counting Detector CT Virtual Monoenergetic Images for Coronary Artery Stenosis Quantification: Phantom and In Vivo Evaluation"

Aus urheberrechtlichen Gründen wurde der Artikel nicht in die vorliegende Dissertation aufgenommen. Siehe Originalpublikation:

Wolf EV, Halfmann MC, Varga-Szemes A, Fink N, Kloeckner R, Bockius S, Allmendinger T, Hagenauer J, Koehler T, Kreitner KF, Schoepf UJ, Münzel T, Düber C, Gori T, Yang Y, Hell MM, Emrich T. Photon-Counting Detector CT Virtual Monoenergetic Images for Coronary Artery Stenosis Quantification: Phantom and In Vivo Evaluation. AJR Am J Roentgenol. 2024 Mar;222(3):e2330481. doi: 10.2214/AJR.23.30481.

2.4 „Photon-counting detector CT-based virtual monoenergetic reconstructions: repeatability and reproducibility of radiomics features of an organic phantom and human myocardium"

Dieses Kapitel basiert auf der bereits veröffentlichten Open-Access-Publikation:

Wolf EV, Müller L, Schoepf UJ, Fink N, Griffith JP 3rd, Zsarnoczay E, Baruah D, Suranyi P, Kabakus IM, Halfmann MC, Emrich T, Varga-Szemes A, O'Doherty J. Photon-counting detector CT-based virtual monoenergetic reconstructions: repeatability and reproducibility of radiomics features of an organic phantom and human myocardium. Eur Radiol Exp. 2023 Oct 25;7(1):59. doi: 10.1186/s41747-023-00371-8.

Die Publikation wird in der vorliegenden Dissertation gemäß den Bedingungen der Creative Commons Attribution 4.0 International License (CC BY 4.0) nachgenutzt.

Wolf *et al. European Radiology Experimental* (2023) 7:59
https://doi.org/10.1186/s41747-023-00371-8

European Radiology EXPERIMENTAL

ORIGINAL ARTICLE Open Access

Photon-counting detector CT-based virtual monoenergetic reconstructions: repeatability and reproducibility of radiomics features of an organic phantom and human myocardium

Elias V. Wolf[1,2], Lukas Müller[1], U. Joseph Schoepf[2], Nicola Fink[2,3], Joseph P. Griffith III[2], Emese Zsarnoczay[2,4], Dhiraj Baruah[2], Pal Suranyi[2], Ismael M. Kabakus[2], Moritz C. Halfmann[1,5], Tilman Emrich[1,2,5*], Akos Varga-Szemes[2] and Jim O'Doherty[2,6]

Abstract

Background Photon-counting detector computed tomography (PCD-CT) may influence imaging characteristics for various clinical conditions due to higher signal and contrast-to-noise ratio in virtual monoenergetic images (VMI). Radiomics analysis relies on quantification of image characteristics. We evaluated the impact of different VMI reconstructions on radiomic features in *in vitro* and *in vivo* PCD-CT datasets.

Methods An organic phantom consisting of twelve samples (four oranges, four onions, and four apples) was scanned five times. Twenty-three patients who had undergone coronary computed tomography angiography on a first generation PCD-CT system with the same image acquisitions were analyzed. VMIs were reconstructed at 6 keV levels (40, 55, 70, 90, 120, and 190 keV). The phantoms and the patients' left ventricular myocardium (LVM) were segmented for all reconstructions. Ninety-three original radiomic features were extracted. Repeatability and reproducibility were evaluated through intraclass correlations coefficient (ICC) and *post hoc* paired samples ANOVA *t* test.

Results There was excellent repeatability for radiomic features in phantom scans (all ICC = 1.00). Among all VMIs, 36/93 radiomic features (38.7%) in apples, 28/93 (30.1%) in oranges, and 33/93 (35.5%) in onions were not significantly different. For LVM, the percentage of stable features was high between VMIs ≥ 90 keV (90 *versus* 120 keV, 77.4%; 90 *versus* 190 keV, 83.9%; 120 *versus* 190 keV, 89.3%), while comparison to lower VMI levels led to fewer reproducible features (40 *versus* 55 keV, 8.6%).

Conclusions VMI levels influence the stability of radiomic features in an organic phantom and patients' LVM; stability decreases considerably below 90 keV.

Relevance statement Spectral reconstructions significantly influence radiomic features *in vitro* and *in vivo*, necessitating standardization and careful attention to these reconstruction parameters before clinical implementation.

This article belongs to the thematic series entitled "Photon-counting CT: a disrupting innovation in medical imaging" (Guest Editors: Tilman Emrich (Mainz/Germany) and Akos Varga-Szemes (Charleston/US)).

*Correspondence:
Tilman Emrich
Tilman.Emrich@unimedizin-mainz.de
Full list of author information is available at the end of the article

Key points

- Radiomic features have an excellent repeatability within the same PCD-CT acquisition and reconstruction.
- Differences in VMI lead to decreased reproducibility for radiomic features.
- VMI ≥ 90 keV increased the reproducibility of the radiomic features.

Keywords Myocardium, Phantoms (imaging), Radiomics, Reproducibility of results, Tomography (x-ray, computed)

Graphical Abstract

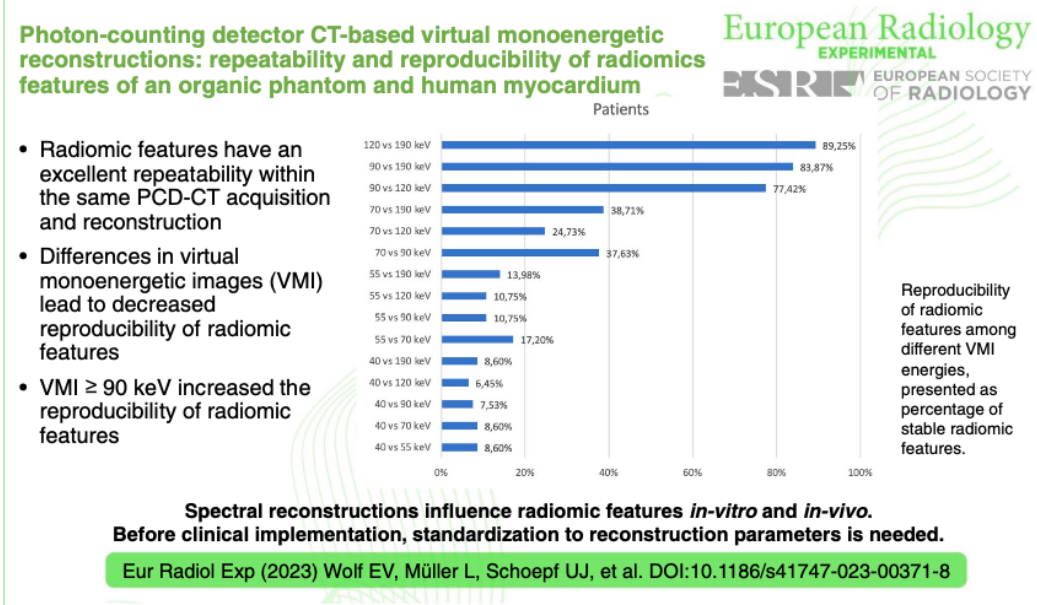

Background

Radiomics is a field of medical imaging that involves the extraction and analysis of quantitative features from medical images, such as computed tomography (CT), magnetic resonance imaging, or positron emission tomography [1, 2]. In combination with machine learning algorithms, radiomics data can be used to provide inferences about tumor characteristics and correlate them with tumor histopathology [3, 4]. Furthermore, radiomic features can be used as biomarkers in oncologic treatment for improved accuracy of prognosis [5–7] and better outcome prediction [8–10], based on machine learning classification models.

In conventional CT imaging, only one image is traditionally formed, which is generated as the average energy of the x-ray spectrum. Dual energy CT (DECT), however, utilizes data acquired at two distinct energy levels to create images that highlight different tissue attenuation properties. The generation of other DECT specific image datasets such as virtual monoenergetic images (VMI), generated at specific energies in the x-ray spectrum) enable the reduction of beam-hardening artifacts and the improvement of the contrast-to-noise ratio [11]. However, such advanced reconstruction was rarely used for cardiac applications due to the limited temporal resolution of the DECT systems. With the recent introduction of a first-generation clinical photon-counting detector CT (PCD-CT) system, spectral imaging based VMI datasets are available by default, without the temporal resolution penalty.

The influence of VMI on the repeatability and reproducibility of radiomic features on energy-integrating detector (EID)-based DECT has previously been investigated [12]. Euler et al. [12] demonstrated in organic phantoms a high repeatability when CT scan settings and reconstructions were kept constant. However, the reproducibility decreased with a larger difference between the two VMI reconstructions being compared. The influence of different VMI has also previously been explored in oncology, including for cervical lymphadenopathy [13, 14], parotid tumors [15], pancreatic tumors [16], and liver lesions [12]. Accordingly, the refinement of VMI could improve the detection and evaluation of several malignant lesions.

Therefore, the aim of this study was to evaluate the impact of different VMI reconstructions on radiomic features in *in vitro* and *in vivo* PCD-CT datasets.

Methods

Phantom study

In order to verify consistency and stability in our radiomic analysis pipeline, phantom experiments were conducted prior to clinical studies. The phantom consisted of twelve organic phantoms (four oranges, four onions, and four apples). Four organic samples of the same item were used to verify radiomic feature extraction repeatability and to identify errors that may be associated with analysis of a specific feature of interest. All objects were placed and fixed on a radiolucent stretcher prior to scanning (Fig. 1).

Phantom data acquisition and reconstruction parameters

Phantom images were acquired on a PCD-CT system (NAEOTOM Alpha, Siemens Healthineers, Forchheim, Germany). The two photon-counting cadmium telluride, CdTe, detectors in the PCD-CT system, each with a nominal 144 × 0.4 mm collimation, enable the acquisition of spectral CT data with a maximum temporal resolution of 66 ms. A standard coronary CT angiography (CCTA) protocol was used in sequential mode with a slice thickness of 0.6 mm, increment of 0.6 mm, and a manually set tube voltage of 120 kVp. Tube current was set to 120 mAs with a resulting volume CT dose index ($CTDI_{vol}$) of 9.45 mGy. A signal mimicking an electrocardiogram was generated to reflect a heart rate of 60 beats per minute, and the examination was initiated during the diastolic phase (75% of the cardiac cycle). All twelve organic phantoms were measured five times to account for the scanner's variability, each time shifting by approximately 2 mm and rotating by approximately 2° [17].

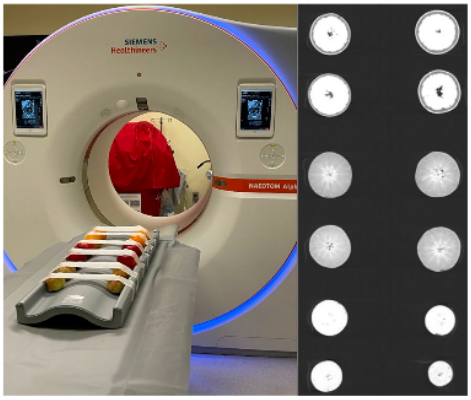

Fig. 1 Phantom setup (left) and a cross-sectional PCD-CT image (right) of the fruit samples reconstructed at 70 keV (window level W1200/C-600)

Images were reconstructed using a quantitative reconstruction kernel (Qr36), quantum iterative reconstruction (QIR) level of 3, a matrix size of 512 with a reconstructed field of view of 750 mm × 200 mm (so that all samples were in the same field of view), and a slice thickness of 0.6 mm. VMIs were reconstructed at six different energies (40, 55, 70, 90, 120, and 190 keV). Detailed acquisition and reconstruction parameters are shown in Table 1.

Patient study

Patient data used in this study was acquired as part of a larger prospective study evaluating PCD-CT for cardiovascular applications. All participants gave written informed consent, and the study protocol was approved by the local Institutional Review Board in accordance with the HIPAA guidelines. Patients were enrolled for this research study based on the following inclusion criteria: (1) individuals who underwent electrocardiographically gated cardiac imaging due to a clinical indication of chest pain; (2) age above 18 years old; (3) no allergy to iodine-based contrast media; (4) intact kidney function with a glomerular filtration rate higher than 45 mL/min/m^2; (5) not currently pregnant or lactating; and (6) able to provide consent. Patients who did not meet all of the inclusion criteria or refused consent were excluded from the study.

Table 1 PCD-CT acquisition and reconstruction parameters

	Phantoms	Patients
Tube potential (kVp)	120	120
Quantum Iterative Reconstruction level	3	3
Reconstruction kernel	Qr36	Qr36
Slice thickness/increment (mm)	0.6/0.6	0.6/0.6
Field of view (mm)	750 × 250	200 × 200
Matrix size	512 × 512	512 × 512
Monoenergetic levels (keV)	40, 55, 70, 90, 120, and 190	40, 55, 70, 90, 120, and 190

Patient data acquisition and image reconstruction

The phantom data acquisition parameters were matched to the acquired patient CCTA scans. A sequential cardiac protocol was used for all CCTA scans, which included ECG triggering and a triphasic contrast injection protocol. This involved injecting an initial bolus of nonionic iodinated contrast agent (50 mL, iopromide 350 mgI/ml; Ultravist, Bayer, Leverkusen, Germany), followed by a 50% mixture of contrast and saline (20 mL), and a saline chaser (25 mL). The injection rate was consistent for all three phases (4 mL/s). If it was not clinically contraindicated, patients were given 0.4 mg nitroglycerin approximately 5 min before the scan, and those with heart rates above 70 beats per minute received 5 mg metoprolol intravenously.

Reconstruction parameters were also identical to the phantom experiment, except for the reduced field of view (200 × 200 mm) limited to the heart.

Image analysis

Digital Imaging and Communications in Medicine, DICOM, images from phantom and patient scans were analyzed using a single radiomic analysis pipeline. Both sets of data were reformatted with 5.0-mm slice thickness and 5.0-mm increment, as is common process in radiomic analysis [18, 19]. The phantom images were loaded into an open-source software (3D Slicer, Version 4.11).

The organic phantoms were semiautomatically segmented with a grow-from-seeds algorithm for each sample group at the 70 keV level. This algorithm was chosen for the phantom images to ensure an accurate and easy workflow. A three-dimensional volume of interest (VOI) of the organic phantoms was generated after applying the algorithm. Each sample was analyzed within their three groups (apples, oranges, and onions). All segmentations were performed on the 70 keV image series, and the VOIs were transferred to the remaining image series (40, 55, 90, 120, and 190 keV). The same procedure was performed for the other four repeated scans.

Additionally, the patient scans were re-orientated on a short-axis view of the left ventricle and simultaneously reformatted according to the phantom study. The six VMI datasets were imported into 3D Slicer. The left ventricular myocardium (LVM) was manually segmented in single slice at the middle of the short-axis stack. The segmented area excluded the trabeculations and papillary muscles (Fig. 2). Segmentation was performed by a reader with 2 years of experience in cardiovascular radiology under the supervision of a board-certified cardiovascular radiologist with 12 years of experience. As in the phantom data, segmentations were performed on the 70 keV image, and the resulting VOIs were transferred to the other five VMI datasets.

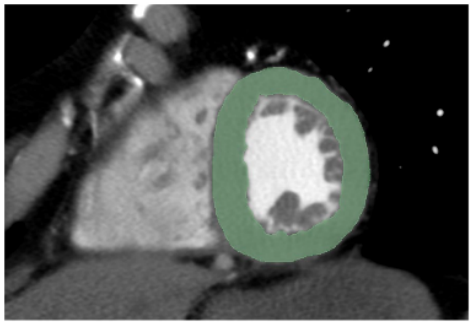

Fig. 2 Representative example of myocardial segmentation in a patient PCD-CT scan at 70 keV

Feature extraction

For extraction, a total of 93 radiomic features were generated in an open source-software (SlicerRadiomics, Pyradiomics, version 3.0.1) with the following feature classes specific to the analysis software: First Order (FO), Gray Level Co-occurrence Matrix (GLCM), Gray Level Dependence Matrix (GLDM), Gray Level Run Length Matrix (GLRLM), Gray Level Size Zone Matrix (GLSZM), and Neighboring Gray Tone Difference Matrix-Features (NGTDM). A standard output from Pyradiomics provides a total of 107 radiomic features. The feature class shape (14 features) was excluded in this analysis because all shape parameters were identical through the transfer from the 70 keV level segmentation to the remaining reconstructions. A full mathematical description of these feature families and representative features within them is available in the software documentation [20]. All 93 radiomic features were extracted for the six different VMIs. From all the segmentations in the phantoms and patients, we analyzed a total of 21,204 radiomic features. The normalized feature values between the range 0 and 1 were calculated by:

$$F_n[i] = \frac{F[i] - F_{min}}{F_{max} - F_{min}}$$

where F[i], Fmin and Fmax represent measured, minimum and maximum value of radiomic feature respectively. The normalized radiomic features were analyzed in their sample groups for the five repeated scans.

Data analysis of repeatability and reproducibility

Radiomic features were considered stable if *post hoc* tests from univariate analysis of variance did not reveal significant differences between VMIs. Repeatability was defined as feature stability between five repeated

phantom scans with the same reconstruction settings. While reproducibility was the feature stability calculated between different VMIs in the same scan (phantom or patient, respectively). The percentage of stable radiomic features of all 93 tested features was used for reporting repeatability or reproducibility.

Furthermore, for reproducibility, the percentage deviation of the normalized values from different VMIs were compared to the normalized values from the lowest VMI (40 keV) in our study.

From previous literature, twelve radiomic features have demonstrated stability between VMIs ranging from 40 to 120 keV on PCD-CT scans between different organs (firstorder_Entropy, glcm_Differenceentropy, glcm_Jointentropy, gldm_DependenceEntropy, gldm_DependenceNonUniformity, gldm_DependenceNonUniformityNormalized, gldm_GrayLevelNonUniformity, glrlm_GrayLevelNonUniformity, glrlm_RunLengthNonUniformity, glrlm_RunLengthNonUniformityNormalized, glrlm_ShortRunEmphasis, ngtdm_Coarseness) [21]. We also specifically examined these preselected features according to our phantom study via intraclass correlation coefficients (ICC) calculations.

Statistical analysis

Statistical analysis was performed with software packages (SPSS Statistics, version 21.0, IBM Corp Armonk, NY; R, version 4.2.2, The R Foundation for Statistical Computing, Vienna, Austria with RStudio, 2022.07.2, Boston, MA, USA with the packages tidyverse [22] and ggplot2 [23], and Excel, version 16.64, Microsoft Corporation, Redmond, WA). For normally distributed data, tested with the Kolmogorov-Smirnov test, mean ± standard deviation was utilized, while for non-normally distributed data, median with interquartile range was utilized. Variables classified as categorical were presented as frequencies and proportions. The difference between radiomic features were compared with a paired samples ANOVA t-test and the corresponding post hoc tests. A p value ≤ 0.05 was considered as statistically significant difference and therefore interpreted as unstable feature between different VMIs. Two-way mixed ICC was used to assess the degree of agreement between distinct VMIs, and the agreement was interpreted as follows: ≤ 0.39, poor agreement; 0.4 to 0.59, moderate agreement; 0.6 to 0.74, good agreement; and ≥ 0.75 excellent agreement [24, 25].

Results

Phantom repeatability analysis

In a logarithmic boxplot, all 93 radiomic features from the three different organic phantoms and five repeated scans showed no significant differences to each other (Fig. 3). Respective ICCs across all VMIs yielded excellent values in repeatability between the different scans (apples ICC = 1.00, oranges ICC = 1.00, and onions

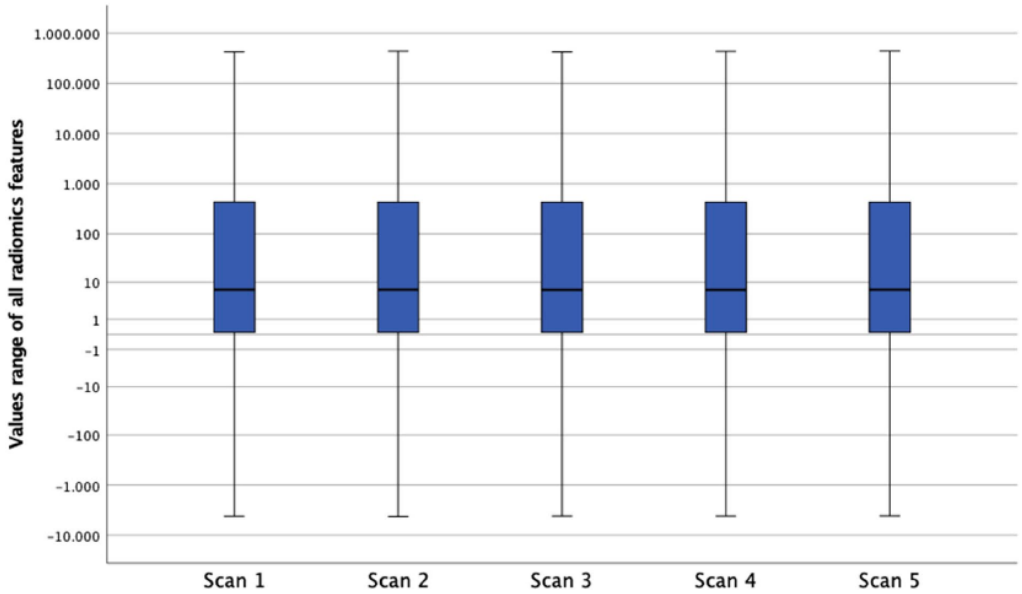

Fig. 3 Logarithmically scaled box plots showing repeatability of radiomic features between the five phantom scans

ICC = 1.00). Additionally, the repeatability for the 70 keV VMI for all three samples over the five repeated scans is shown through scatter plots (Supplemental Figure S1).

Phantom reproducibility analysis

The different samples did not show a substantial reproducibility among the different VMIs (mean reproducibility of all samples: 34.9 %, Fig. 4). The highest values found with 49.5% (apples, 55 *versus* 120 keV), 48.4% (oranges, 120 *versus* 190 keV), and 50.5% (onions, 55 *versus* 120 keV). Additionally, the reproducibility compared to the 40 keV VMI for all three samples is shown in scatter plots (Supplemental Figure S2).

Preselected features reproducibility analysis

The previous described twelve stable radiomic features were tested for reproducibility between six different VMIs on the organic phantom. Excellent agreements with ICC values above 0.75 were seen in comparisons with both VMI ≥ 90 keV. Comparisons of 90 *versus* 120 keV (apples = 11 (91.7%), oranges = 10 (83.3%), onions = 11 (91.7%)), 90 *versus* 190 keV (apples = 11 (91.7%), oranges = 10 (83.3%), onions = 6 (50.0%)), and 120 *versus* 190 keV (apples = 11 (91.7%), oranges = 11 (91.7%), onions = 9 (75.0%)) showed excellent (≥ 0.75) ICC values of the twelve preselected features.

At VMIs ≥ 90 keV (90 *versus* 120 keV, 90 *versus* 190 keV, and 120 *versus* 190 keV), 91.7% of radiomic features were stable, whereas below 90 keV (40 *versus* 70 keV, 40 *versus* 90 keV, 40 *versus* 120 keV, and 40 *versus* 190 keV), only 8.3% were stable. This illustrates a trend that a higher percentage of radiomic features was stable at higher VMIs (≥ 90 keV) and VMIs in close proximity of each other (*i.e.*, 90 *versus* 120 keV: 32/36, 88.9%) than at VMIs with a greater keV difference (*i.e.*, 40 *versus* 120 keV: 4/36, 11.1%). The summation/percentage values (Table 2) and the individual values (Supplemental Table S1) are shown in the corresponding tables.

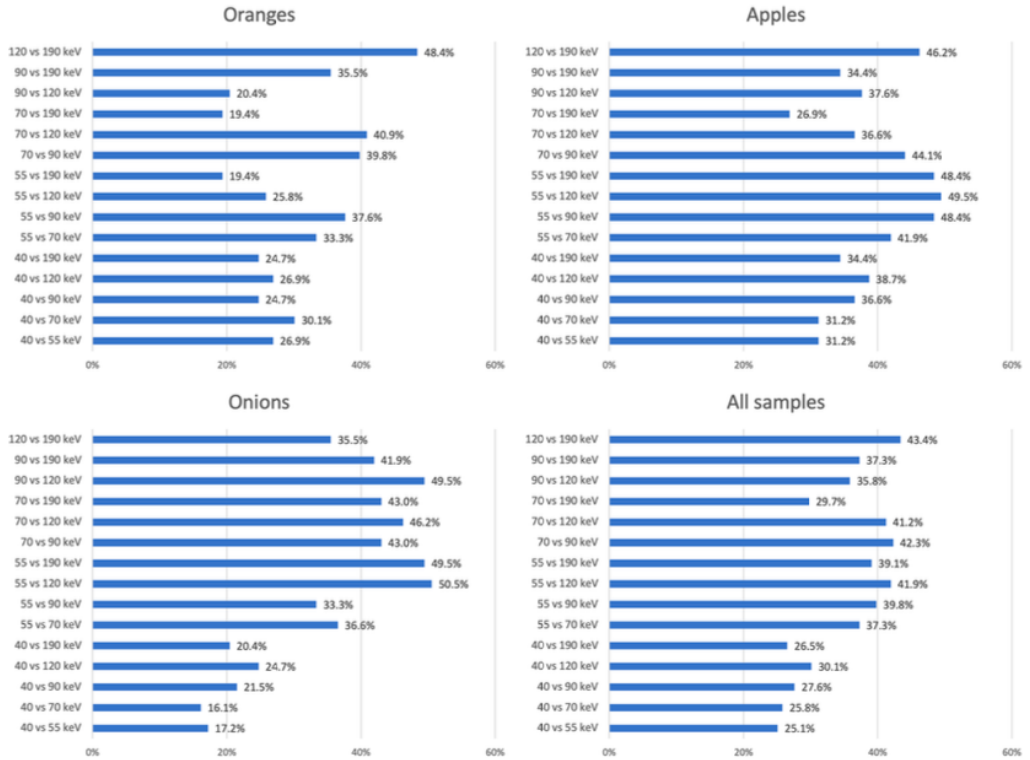

Fig. 4 Reproducibility of radiomic features between different VMI energies (40, 55, 70, 90, 120, and 190 keV) in oranges, onions, apples, and all samples. The values are shown as percentage of stable radiomic features out of all 93 features

Table 2 ICC > 0.75 summation from 12 previously described radiomics features

	40 vs 55	40 vs 70	40 vs 90	40 vs 120	40 vs 190	55 vs 70	55 vs 90	55 vs 120	55 vs 190	70 vs 90	70 vs 120	70 vs 190	90 vs 120	90 vs 190	120 vs 190
Apples	8 (66.7%)	1 (8.3%)	1 (8.3%)	1 (8.3%)	1 (8.3%)	4 (33.3%)	4 (33.3%)	3 (25.0%)	4 (33.3%)	9 (75.0%)	9 (75.0%)	9 (75.0%)	11 (91.7%)	11 (91.7%)	11 (91.7%)
Oranges	6 (50.0%)	4 (33.3%)	2 (16.7%)	2 (16.7%)	3 (25.0%)	4 (33.3%)	3 (25.0%)	2 (16.7%)	4 (33.3%)	7 (58.3%)	7 (58.3%)	9 (75.0%)	10 (83.3%)	10 (83.3%)	11 (91.7%)
Onions	7 (58.3%)	7 (58.3%)	7 (58.3%)	1 (8.3%)	2 (16.7%)	7 (58.3%)	8 (66.7%)	4 (33.3%)	4 (33.3%)	8 (66.7%)	2 (16.7%)	3 (25.0%)	11 (91.7%)	6 (50.0%)	9 (75.0%)
Total	21 (58.3%)	12 (33.3%)	10 (27.8%)	4 (11.1%)	6 (16.7%)	15 (41.7%)	15 (41.7%)	9 (25.0%)	12 (33.3%)	24 (66.7%)	18 (50.0%)	21 (58.3%)	32 (88.9%)	27 (75.0%)	31 (86.1%)

Myocardium reproducibility analysis

The study population included a total of 23 patients (16 men, 69.6 %) with an average age of 65 ± 12 years (mean ± standard deviation). The radiation dose of the CCTA scan had a median $CTDI_{vol}$ of 24.0 (interquartile range 17.7–50.4) mGy. Details of the study population are given in Table 3.

The patient cohort also showed a higher percentage of stable radiomic features between VMI energies comparisons ≥ 90 keV (90 *versus* 120 keV, 77.4%, 90 *versus* 190 keV, 83.9%; and 120 *versus* 190 keV, 89.3%). This trend decreased with lower VMIs down to 6.5% (40 *versus* 120 keV, Fig. 5). Close proximity of VMIs did not always lead to a higher ICC result (*e.g.*, 40 *versus* 55 keV, 8.6%).

Table 3 Patient characteristics

N	23
Female (%)	7 (30.4)
Age (years)	65 ± 12.1
BMI (kg/m^2)	30.1 ± 7.1
Heart rate (bpm)	65.3 ± 10.8
$CTDI_{vol}$ (mGy)	24.0 (17.7–50.4)
DLP (mGy*cm)	557.5 ± 384.7

BMI Body mass index, *bpm* Beats per minute, *CTDI* Computer tomography dose index, *DLP* Dose length product, *PCD-CT* Photon-counting detector CT

Values are mean ± standard deviation, median (interquartile range), *n* (frequencies)

Interestingly, the lowest VMI at 40 keV resulted in the lowest correlation values, all under 10% (average 8.0%).

Discussion

This study investigated the difference in radiomic features derived from various VMI reconstructions in an organic phantom and a patient cohort scanned on a PCD-CT system. The major findings were the following. First, radiomic features had an excellent repeatability (ICC = 1.00) in organic phantoms when using the same acquisition and reconstruction parameters. Second, while the comparison of different VMIs showed inconsistent reproducibility of radiomic features in the organic phantom samples, there was a higher reproducibility between higher VMIs (90, 120, and 190 keV) in twelve preselected radiomic features, as well as in the patient cohort. Third, VMIs < 90 keV result in decreased ICC values, which should be considered while using radiomic features. The knowledge gained from these findings could guide VMI choice in further clinical studies of radiomic features.

By demonstrating almost perfect repeatability of radiomic features within the same VMI, our phantom study indicates that radiomic features are reliable when using the same acquisition and reconstruction parameters. Conversely, reproducibility was low between different VMIs in both the phantom and patient measurements. This finding implies that slight modification of the VMI impacts the characteristics of radiomic features. Furthermore, there

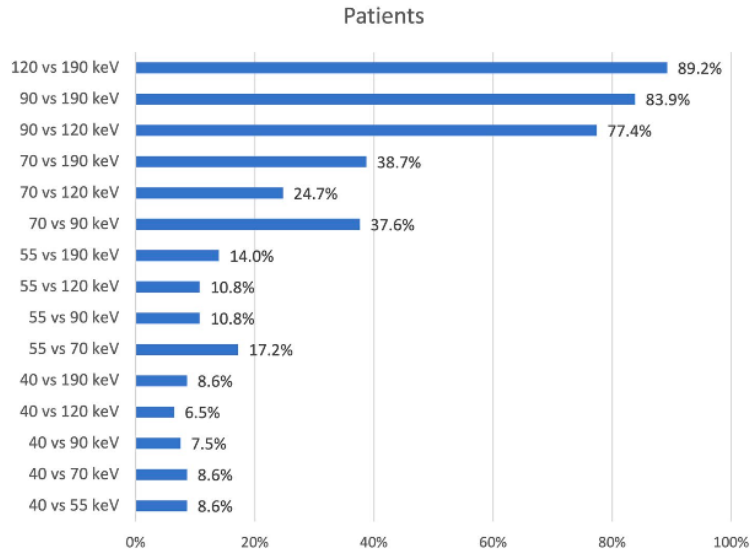

Fig. 5 Reproducibility of radiomic features among different VMI energies (40, 55, 70, 90, 120, and 190 keV) in a single myocardial slice in patients. The values are shown as percentage of stable radiomic features out of all 93 features

was no transferability of the same trend from the phantom to patient's results. A possible reason could be the difference in textures between the organic phantom and the myocardium, especially in the presence of contrast agent. Generally, the agreement between phantom and patient experiments is limited in the context of radiomic features and needs to be explored further. Interestingly, we obtained a stable plateau phase in our patient cohort between VMIs of 90 and 190 keV. A possible explanation would be that iodine, as a contrast agent, is an important factor that influences the radiomic features analysis. At VMIs ≥ 90 keV, there is minimal change in the attenuation coefficient of iodine [26], therefore improved reproducibility of the radiomic features may be observed. On the other hand, this study observed the instability of radiomic features at lower VMIs. At lower VMIs the gap to the attenuation coefficient of iodine is closer and differences in VMIs may have a greater impact on the stability of radiomic features.

Euler et al. [12] investigated the impact of different VMIs on the repeatability and reproducibility of radiomic features in a phantom on a DECT system. According to their results, there was a high repeatability of radiomic features within the same VMI. Repeatability was roughly 80% when acquisition and reconstruction parameters were kept constant. Similar to our study, the reproducibility of radiomic features differed between various VMIs. Increased reproducibility was found in reconstructions with lower keV differences. This trend was not evaluated in our phantom or patient study and could be attributed to several different factors, such as different statistical methods (concordance–correlation–coefficient *versus* ANOVA t-test), different selection of radiomic features (1218 *versus* 93) or different CT scanners (EID-CT *versus* PCD-CT). However, a common conclusion is that the use of different VMIs does not reproduce similar radiomic feature values on EID-CT or PCD-CT.

Mackin et al. [27] investigated inter-scanner variability of radiomic features generated by four different CT vendors. They conducted a phantom study consisting of 10 different materials imaged in 17 different scan modes. The results showed that the variability of radiomic features depended not only on the scanner but also on the acquisition and reconstruction parameters. This study highlights the importance of consistent image settings for the reproducibility of radiomic features on EID-CT, which is supported by other similar studies in the literature [28–33].

While most image settings need to remain constant to achieve high radiomic feature reproducibility, other settings such as tube current can be changed without substantial effect of radiomic feature values. An organic phantom study by Hertel et al. [34] demonstrated a test-retest stability of 75% of the radiomic features between different radiation dose values (10 mAs, 50 mAs, and 100 mAs). Their study demonstrated that reproducibility of radiomic features was not substantially affected by changes in radiation dose.

Conversely, when image settings such as kernel or spatial resolution change, there is a fundamental decrease in radiomic feature reproducibility. For example, Dunning et al. [35] demonstrated that 13 of 14 relevant radiomic features differed by more than 50% between PCD- and EID-CT. Further, Tharmaseelan et al. [21] demonstrated that VMI (40–120 keV in 10 steps) has an important impact on radiomic feature stability in various abdominal tissue (liver, lung, spleen, psoas muscle and subcutaneous fat). Of the 93 features analyzed in their study, only 12 had ICC values ≥ 0.75 in three or more organs. Additionally, different tissues had different features with the best reproducibility. Interestingly, the twelve radiomic features with the highest agreement found in the study by Tharmaseelan et al. [21] did not have high reproducibility in our study. Perhaps this difference was due to different acquisition settings or content of the phantom/tissue being imaged. Overall, understanding the effect of each imaging settings on the reproducibility of radiomic features is critical to gathering information that is ultimately useful in patient management.

Clinical application and clinical decision models may potentially involve radiomic feature assessment in the future. Before the implementation of such models, it is crucial to have a better understanding of the stability of radiomic features and their influence by disruptive factors. Our investigation contributes to this knowledge by exploring the influence of VMIs on the stability of radiomic features in a phantom and in human LVM.

Several limitations should be taken into account when evaluating this investigation. First, a larger patient group would be beneficial in future studies, as our patient cohort was limited to 23 individuals. However, large cohort studies in radiomics are generally rare. Second, patient PCD-CT scans were acquired with a higher radiation dose levels than the phantom PCD-CT scans. Radiation dose was lower for organic phantom scans as we utilized a clinical protocol with automated dose modulation, which resulted in a lower value of mAs. Nevertheless, several aforementioned studies have shown that different radiation dose levels do not change radiomic feature values substantially [12, 35]. Third, the phantom texture materials differ from the myocardial texture with contrast enhanced scans, and therefore the results may not be transferable. Further investigations with native CT scans have to be investigated, which were not available in this study. An improved heart phantom model would be preferable. Fourth, possible variations in heart rate and other acquisition parameters, such as breath-hold and positioning, may have an impact on the patient measurements, but these potential effects were not

explored in the study. Fifth, this study did not investigate the relationship between radiomic features and clinical outcomes, which should be considered in larger clinical studies. This investigation concentrates on the influence of VMIs on the stability of radiomic features. Sixth, intra- and inter-rater reproducibility was not included in the scope of this study and should be highlighted in further clinical investigations. Finally, we considered only examinations from PCD-CT, and these results may not be transferable to other CT scanners. Further studies are needed to evaluate the influence of different scanner types on radiomic features.

In conclusion, VMI influences *in vitro* and *in vivo* characteristics of radiomic features on PCD-CT, resulting in a different rate of reproducibility among different VMI. There seems to be a better correlation of reproducibility between higher VMI in myocardial texture. Further studies are necessary to determine imaging protocols for optimizing radiomic feature stability on PCD-CT.

Abbreviations

CCTA	Coronary CT angiography
CT	Computed tomography
$CTDI_{vol}$	Volume CT dose index
DECT	Dual energy CT
EID	Energy-integrating detector
PCD-CT	Photon-counting detector CT
VMI	Virtual monoenergetic image
VOI	Volume of interest

Supplementary Information

The online version contains supplementary material available at https://doi.org/10.1186/s41747-023-00371-8.

Additional file 1: Supplementary Figure S1. Scatter plot of all 93 normalized radiomics features for the five repeated scans at 70 keV.**Supplementary Figure 2.** Scatter plot of all 93 normalized radiomics features deviation compared to the related normalized radiomics features at 40 keV between -100 and 100%. **Supplementary Table S1.** ICC of 12 previous described stable features between the different VMIs (40, 55, 70, 90, 120, and 190 keV).

Authors' contributions

EVW, LM, MCH, and TE designed the study, interpreted the study data and drafted the manuscript. DB, PS, and IMK acquired data and substantially revised the manuscript. NF, JPG, and EZ performed data analysis, supported statistical analysis, and substantially revised the manuscript. JOD advised data reconstruction, supervised data analysis and edited / revised the manuscript. AV-S and UJS supervised the study conception and data interpretation and substantially edited the manuscript. All authors read and approved the final manuscript.

Funding

Open Access funding enabled and organized by Projekt DEAL. This work was supported by a research grant from Siemens Healthineers. The MAInz-DOC Doctoral College and the Kaltenbach Doctoral Scholarship of the German Heart Foundation supported EVW.

Availability of data and materials

The datasets used and/or analyzed during the current study are available from the corresponding author on reasonable request.

Declarations

Ethics approval and consent to participate

The studies involving human participants were reviewed and approved by Institutional Review Board, Medical University of South Carolina, SC, USA. The patients/participants provided their written informed consent to participate in this study.

Consent for publication

Not applicable

Competing interests

UJS received institutional research support and/or personal fees from Bayer, Bracco, Elucid Bioimaging, Guerbet, HeartFlow, Keya Medical, and Siemens. AV-S is Deputy Editor of *European Radiology Experimental*. He has not taken part in the review or selection process of this article. AV-S received institutional research support and/or personal fees from Elucid Bioimaging and Siemens. TE is a member of the *European Radiology Experimental* Scientific Editorial Board. He has not taken part in the review or selection process of this article. TE received a speaker fee and travel support from Siemens Medical Solutions USA, Inc.
JO'D was an employee of Siemens Medical Solutions USA, Inc.

Author details

[1]Department of Diagnostic and Interventional Radiology, University Medical Center of the Johannes Gutenberg-University, Mainz, Germany. [2]Division of Cardiovascular Imaging, Department of Radiology and Radiological Science, Medical University of South Carolina, Charleston, SC, USA. [3]Department of Radiology, University Hospital, LMU Munich, Munich, Germany. [4]Medical Imaging Centre, Semmelweis University, Budapest, Hungary. [5]German Centre for Cardiovascular Research, Partner site Rhine-Main, Mainz, Germany. [6]Siemens Medical Solutions USA Inc, Malvern, PA, USA.

Received: 12 May 2023 Accepted: 17 July 2023
Published online: 25 October 2023

References

1. Gillies RJ, Kinahan PE, Hricak H (2016) Radiomics: images are more than pictures, they are data. Radiology 278:563–77. https://doi.org/10.1148/radiol.2015151169
2. Mayerhoefer ME, Materka A, Langs G et al (2020) Introduction to radiomics. J Nucl Med 61:488–95. https://doi.org/10.2967/jnumed.118.222893
3. Huang YQ, Liang CH, He L et al (2016) Development and validation of a radiomics nomogram for preoperative prediction of lymph node metastasis in colorectal cancer. J Clin Oncol 34:2157–64. https://doi.org/10.1200/JCO.2015.65.9128
4. Aerts HJ, Velazquez ER, Leijenaar RT et al (2014) Decoding tumour phenotype by noninvasive imaging using a quantitative radiomics approach. Nat Commun 5:4006. https://doi.org/10.1038/ncomms5006
5. Liu Z, Wang S, Dong D et al (2019) The applications of radiomics in precision diagnosis and treatment of oncology: opportunities and challenges. Theranostics 9:1303–22. https://doi.org/10.7150/thno.30309
6. Woznicki P, Westhoff N, Huber T et al. (2020) Multiparametric MRI for prostate cancer characterization: combined use of radiomics model with PI-RADS and clinical parameters. Cancers (Basel) 12. https://doi.org/10.3390/cancers12071767
7. Enke JS, Moltz JH, D'Anastasi M et al. (2022) Radiomics features of the spleen as surrogates for CT-based lymphoma diagnosis and subtype differentiation. Cancers (Basel) 14. https://doi.org/10.3390/cancers14030713
8. Tian X, Sun C, Liu Z et al (2020) Prediction of response to preoperative neoadjuvant chemotherapy in locally advanced cervical cancer using multicenter CT-based radiomic analysis. Front Oncol 10:77. https://doi.org/10.3389/fonc.2020.00077
9. Vaidya P, Bera K, Gupta A et al (2020) CT derived radiomic score for predicting the added benefit of adjuvant chemotherapy following surgery in stage I, II resectable non-small cell lung cancer: a retrospective multicohort study for outcome prediction. Lancet Digit Health 2:e116–e28. https://doi.org/10.1016/s2589-7500(20)30002-9

10. Li H, Zhang R, Wang S et al (2020) CT-based radiomic signature as a prognostic factor in stage IV ALK-positive non-small-cell lung cancer treated with TKI crizotinib: a proof-of-concept study. Front Oncol 10:57. https://doi.org/10.3389/fonc.2020.00057
11. Forghani R, De Man B, Gupta R (2017) Dual-energy computed tomography: physical principles, approaches to scanning, usage, and implementation: part 2. Neuroimaging Clin N Am 27:385–400. https://doi.org/10.1016/j.nic.2017.03.003
12. Euler A, Laqua FC, Cester D et al. (2021) Virtual monoenergetic images of dual-energy CT-impact on repeatability, reproducibility, and classification in radiomics. Cancers (Basel) 13. https://doi.org/10.3390/cancers13184710
13. Forghani R, Chatterjee A, Reinhold C et al (2019) Head and neck squamous cell carcinoma: prediction of cervical lymph node metastasis by dual-energy CT texture analysis with machine learning. Eur Radiol 29:6172–81. https://doi.org/10.1007/s00330-019-06159-y
14. Seidler M, Forghani B, Reinhold C et al (2019) Dual-energy CT texture analysis with machine learning for the evaluation and characterization of cervical lymphadenopathy. Comput Struct Biotechnol J 17:1009–15. https://doi.org/10.1016/j.csbj.2019.07.004
15. Al Ajmi E, Forghani B, Reinhold C et al (2018) Spectral multi-energy CT texture analysis with machine learning for tissue classification: an investigation using classification of benign parotid tumours as a testing paradigm. Eur Radiol 28:2604–11. https://doi.org/10.1007/s00330-017-5214-0
16. An C, Li D, Li S et al (2022) Deep learning radiomics of dual-energy computed tomography for predicting lymph node metastases of pancreatic ductal adenocarcinoma. Eur J Nucl Med Mol Imaging 49:1187–99. https://doi.org/10.1007/s00259-021-05573-z
17. Groen JM, Greuter MJ, Vliegenthart R et al (2008) Calcium scoring using 64-slice MDCT, dual source CT and EBT: a comparative phantom study. Int J Cardiovasc Imaging 24:547–56. https://doi.org/10.1007/s10554-007-9282-0
18. Ayx I, Tharmaseelan H, Hertel A et al. (2022) Comparison study of myocardial radiomics feature properties on energy-integrating and photon-counting detector CT. Diagnostics (Basel) 12. https://doi.org/10.3390/diagnostics12051294
19. Lohmann P, Bousabarah K, Hoevels M et al (2020) Radiomics in radiation oncology-basics, methods, and limitations. Strahlenther Onkol 196:848–55. https://doi.org/10.1007/s00066-020-01663-3
20. van Griethuysen JJM, Fedorov A, Parmar C et al (2017) Computational radiomics system to decode the radiographic phenotype. Cancer Res 77:e104–e7. https://doi.org/10.1158/0008-5472.CAN-17-0339
21. Tharmaseelan H, Rotkopf LT, Ayx I et al (2022) Evaluation of radiomics feature stability in abdominal monoenergetic photon counting CT reconstructions. Sci Rep 12:19594. https://doi.org/10.1038/s41598-022-22877-8
22. Wickham H, Averick M, Bryan J et al. (2019) Welcome to the tidyverse. Journal of Open Source Software 4. https://doi.org/10.21105/joss.01686
23. Wickham H (2016) ggplot2: elegant graphics for data analysis. Springer-Verlag, New York
24. Khan JN, Singh A, Nazir SA et al (2015) Comparison of cardiovascular magnetic resonance feature tracking and tagging for the assessment of left ventricular systolic strain in acute myocardial infarction. Eur J Radiol 84:840–8. https://doi.org/10.1016/j.ejrad.2015.02.002
25. Baessler B, Weiss K, Pinto Dos Santos D (2019) Robustness and reproducibility of radiomics in magnetic resonance imaging: a phantom study. Invest Radiol 54:221–8. https://doi.org/10.1097/RLI.0000000000000530
26. Emrich T, O'Doherty J, Schoepf UJ et al (2023) Reduced iodinated contrast media administration in coronary CT angiography on a clinical photon-counting detector CT system: a phantom study using a dynamic circulation model. Invest Radiol 58:148–55. https://doi.org/10.1097/RLI.0000000000000911
27. Mackin D, Fave X, Zhang L et al (2015) Measuring computed tomography scanner variability of radiomics features. Invest Radiol 50:757–65. https://doi.org/10.1097/RLI.0000000000000180
28. Berenguer R, Pastor-Juan MDR, Canales-Vazquez J et al (2018) Radiomics of CT features may be nonreproducible and redundant: influence of CT acquisition parameters. Radiology 288:407–15. https://doi.org/10.1148/radiol.2018172361
29. Mannil M, von Spiczak J, Muehlematter UJ et al (2019) Texture analysis of myocardial infarction in CT: comparison with visual analysis and impact of iterative reconstruction. Eur J Radiol 113:245–50. https://doi.org/10.1016/j.ejrad.2019.02.037
30. Milanese G, Mannil M, Martini K et al (2019) Quantitative CT texture analysis for diagnosing systemic sclerosis: effect of iterative reconstructions and radiation doses. Medicine (Baltimore) 98:e16423. https://doi.org/10.1097/MD.0000000000016423
31. Meyer M, Ronald J, Vernuccio F et al (2019) Reproducibility of CT radiomic features within the same patient: influence of radiation dose and CT reconstruction settings. Radiology 293:583–91. https://doi.org/10.1148/radiol.2019190928
32. van Timmeren JE, Cester D, Tanadini-Lang S et al (2020) Radiomics in medical imaging-"how-to" guide and critical reflection. Insights Imaging 11:91. https://doi.org/10.1186/s13244-020-00887-2
33. Park BW, Kim JK, Heo C et al (2020) Reliability of CT radiomic features reflecting tumour heterogeneity according to image quality and image processing parameters. Sci Rep 10:3852. https://doi.org/10.1038/s41598-020-60868-9
34. Hertel A, Tharmaseelan H, Rotkopf LT et al (2023) Phantom-based radiomics feature test-retest stability analysis on photon-counting detector CT. Eur Radiol. https://doi.org/10.1007/s00330-023-09460-z
35. Dunning CAS, Rajendran K, Fletcher JG et al. (2022) Impact of improved spatial resolution on radiomic features using photon-counting-detector CT. Proc SPIE Int Soc Opt Eng 12032. https://doi.org/10.1117/12.2612229

Publisher's Note

3 Diskussion

Zusammenfassend zeigen die einzelnen Veröffentlichungen, dass die PCD-CT die Beurteilung der kardialen Strukturen beeinflusst.

Im intraindividuellen Vergleich zwischen PCD- und EID-CT erbrachte die PCD-CT tendenziell niedrigere Kalzium-Score Werte und ermittelte das Kalzium-Volumen genauer als die EID-CT. Dies führte zu einer potenziell niedrigeren Risikoklassifizierung von 5,25% der Patienten, die einen Kalzium-Score durch die EID-CT erhielten. Auch im intraindividuellen Stenosenvergleich zwischen PCD- und EID-CT erbrachte die PCD-CT tendenziell niedrigere PDS-Werte. Dadurch verbunden kam es zu einer potenziell niedrigeren CAD-RADS Klassifizierung von 17,4% der Patienten. Zudem konnte gezeigt werden, dass unterschiedliche VMI Level in der PCD-CT einen Einfluss auf die Stenosequantifizierung haben. Höhere VMI Level steigerten die Genauigkeit bei der Bewertung von kalzifizierten (100 keV) und gemischten (140 keV) Plaques, während niedrigere VMI Level (40 keV) sich besser für die Beurteilung von nicht-kalzifizierten Plaques eigneten. Blooming-Artefakte verringerten sich bei kalzifizierten und gemischten Plaques durch das Erhöhen der VMI Level.

Ebenfalls wurde die Variabilität von Radiomics-Merkmalen durch unterschiedliche VMI Level in der PCD-CT beeinflusst. Dabei zeigte sich eine exakte Reliabilität bei gleichen Akquisitions- und Rekonstruktionsparametern. Bei unterschiedlichen VMI Leveln verringerte sich jedoch erheblich die Reproduzierbarkeit. Dies legt nahe, dass bereits leichte Anpassungen der VMI Level signifikante Auswirkungen auf die Charakteristiken der Radiomics-Merkmale haben. Allerdings wurde eine verbesserte Reproduzierbarkeit zwischen höheren VMI Leveln (90, 120 und 190 keV) beobachtet.

Die Verwendung einer PCD-CT in Kombination mit spezifischen VMI Leveln kann zu einer präziseren Quantifizierung von kardialen Strukturen, insbesondere der Koronargefäße, führen. Die Relevanz der CCTA für die klinische Risikobewertung und den Entscheidungsfindungsprozess lässt sich dadurch steigern. Dies konnte durch die beschriebenen Ergebnisse gezeigt und evaluiert werden. Dennoch sind weitere klinische Studien notwendig, um optimale Protokolle für die PCD-CT zu entwickeln und deren Einfluss auf die Risikoklassifizierung sowie die Ableitung von Therapieempfehlungen für Patienten genauer zu bestimmen.

Zudem wird aktuell an weiteren Rekonstruktionsmöglichkeiten geforscht, um eine genauere Stenosemessung zu ermöglichen. Ein innovativer Bildrekonstruktionsalgorithmus, wie Virtual Non-Calcium (VNCa), könnte die Genauigkeit der Stenosebeurteilung in der PCD-CT signifikant erhöhen. Dadurch werden kalkhaltige Plaques virtuell subtrahiert und das kontrastmittelgefüllte Gefäß besser sichtbar gemacht. Allmendinger et al. haben diese

Methode bereits in einer Phantomstudie untersucht und festgestellt, dass VNCa-Rekonstruktionen eine präzisere Stenoseklassifizierung ermöglichen als die herkömmliche monoenergetische Rekonstruktion in der PCD-CT (27). Zudem verdeutlichte sich auch in einer Studienkohorte, dass VNCa-Rekonstruktionen, anders als VMI-Rekonstruktionen im Vergleich zur QCA keine Überschätzung von Stenosen erzielten (28).

Die Stenosebewertung kann in Zukunft durch die Anwendung des Ultra-high Resolution (UHR) Modus (0,2 mm Schichtdicke) der PCD-CT verbessert werden. Durch die höhere räumliche Auflösung kann das Kalzium-Blooming verringert und somit die Bildqualität von starken Verkalkungen erhöht werden. In dynamischen Phantomexperimenten führten UHR-Rekonstruktionen zu präziseren Stenosequantifizierungen im Vergleich zu Aufnahmen mit der Standardauflösung (0,6 mm Schichtdicke) (29). Die erhöhte diagnostische Präzision von UHR konnte auch in Patientenstudien belegt werden. Die UHR-CCTA identifizierte Stenosen (≥ 50%) im Vergleich zur ICA mit einer Sensitivität von 96% (30). Eine weitere Patientenstudie unterstrich die genauere Stenosequantifizierung mittels UHR verglichen zur Standardauflösung. Dieser Unterschied führte zu einer Reklassifizierung von rund 54% der Patienten in eine niedrigere CAD-RADS Klasse (31). Zukünftige Studien sind erforderlich, um VMI und UHR im Kontext der Stenosebeurteilung zu vergleichen und somit ein besseres Verständnis dieser beiden Rekonstruktionsmethoden zu gewinnen. Künftige Updates der PCD-CT sollen sicherstellen, dass UHR-, VMI- und VNCa-Rekonstruktionen standardmäßig nach jedem CT-Scan verfügbar sind. Derzeit ist es noch nicht möglich, spektrale EKG-getriggerte Daten in UHR-Auflösung zu erzeugen.

Jedoch weist UHR bestimmte Nachteile auf wie eine höhere Strahlenexposition und eine eingeschränkte Abdeckung in z-Richtung. Eine vorherige Studie zeigte, dass zur Erzielung der gleichen Kontrastauflösung mit UHR im Vergleich zur Standardauflösung eine 23% höhere Strahlendosis erforderlich ist (32). Daraus ergibt sich, dass UHR bei jungen Patienten und bei Patienten mit nur geringfügigen oder nicht-kalzifizierten Plaques, nicht angewendet werden sollte. Aufgrund der geringeren z-Coverage treten zudem vermehrt Step-Artefakte auf, die jedoch durch neuartige Algorithmen verhindert werden können (33).

Insgesamt zeigt sich, dass die Anwendung der PCD-CT und optimierter VMI Level einen klaren Vorteil in der Herzbildgebung bietet und somit eine verbesserte Einschätzung der Kalzifizierungen in der KHK ermöglicht.

4 Literaturverzeichnis

1. Malakar AK, Choudhury D, Halder B, Paul P, Uddin A, Chakraborty S. A review on coronary artery disease, its risk factors, and therapeutics. J Cell Physiol. 2019;234(10):16812-23.
2. Moss AJ, Williams MC, Newby DE, Nicol ED. The Updated NICE Guidelines: Cardiac CT as the First-Line Test for Coronary Artery Disease. Curr Cardiovasc Imaging Rep. 2017;10(5):15.
3. Knuuti J, Wijns W, Saraste A, Capodanno D, Barbato E, Funck-Brentano C, et al. 2019 ESC Guidelines for the diagnosis and management of chronic coronary syndromes. Eur Heart J. 2020;41(3):407-77.
4. Willemink MJ, Persson M, Pourmorteza A, Pelc NJ, Fleischmann D. Photon-counting CT: Technical Principles and Clinical Prospects. Radiology. 2018;289(2):293-312.
5. Flohr T, Petersilka M, Henning A, Ulzheimer S, Ferda J, Schmidt B. Photon-counting CT review. Phys Med. 2020;79:126-36.
6. van der Bie J, van Straten M, Booij R, Bos D, Dijkshoorn ML, Hirsch A, et al. Photon-counting CT: Review of initial clinical results. Eur J Radiol. 2023;163:110829.
7. Mergen V, Eberhard M, Manka R, Euler A, Alkadhi H. First in-human quantitative plaque characterization with ultra-high resolution coronary photon-counting CT angiography. Front Cardiovasc Med. 2022;9:981012.
8. Mergen V, Sartoretti T, Baer-Beck M, Schmidt B, Petersilka M, Wildberger JE, et al. Ultra-High-Resolution Coronary CT Angiography With Photon-Counting Detector CT: Feasibility and Image Characterization. Invest Radiol. 2022;57(12):780-8.
9. Vattay B, Szilveszter B, Boussoussou M, Vecsey-Nagy M, Lin A, Konkoly G, et al. Impact of virtual monoenergetic levels on coronary plaque volume components using photon-counting computed tomography. Eur Radiol. 2023;33(12):8528-39.
10. Zsarnoczay E, Varga-Szemes A, Emrich T, Szilveszter B, van der Werf NR, Mastrodicasa D, et al. Characterizing the Heart and the Myocardium With Photon-Counting CT. Invest Radiol. 2023;58(7):505-14.
11. Divakaran S, Cheezum MK, Hulten EA, Bittencourt MS, Silverman MG, Nasir K, et al. Use of cardiac CT and calcium scoring for detecting coronary plaque: implications on prognosis and patient management. Br J Radiol. 2015;88(1046):20140594.

12. Biavati F, Saba L, Boussoussou M, Kofoed KF, Benedek T, Donnelly P, et al. Coronary Artery Calcium Score Predicts Major Adverse Cardiovascular Events in Stable Chest Pain. Radiology. 2024;310(3):e231557.

13. Tummala R, Han D, Friedman J, Hayes S, Thomson L, Gransar H, et al. Association between plaque localization in proximal coronary segments and MACE outcomes in patients with mild CAC: Results from the EISNER study. Am J Prev Cardiol. 2022;12:100423.

14. Vakil P, Wen Z, Lima AS, Weber EJ, Kallianos KG, Elicker BM, et al. Predictive Value of Coronary Artery Calcium in Patients Receiving Computed Tomography Pulmonary Angiography for Suspected Pulmonary Embolism in the Emergency Department. J Thorac Imaging. 2022;37(5):279-84.

15. Arnett DK, Blumenthal RS, Albert MA, Buroker AB, Goldberger ZD, Hahn EJ, et al. 2019 ACC/AHA Guideline on the Primary Prevention of Cardiovascular Disease: Executive Summary: A Report of the American College of Cardiology/American Heart Association Task Force on Clinical Practice Guidelines. J Am Coll Cardiol. 2019;74(10):1376-414.

16. Obisesan OH, Osei AD, Uddin SMI, Dzaye O, Blaha MJ. An Update on Coronary Artery Calcium Interpretation at Chest and Cardiac CT. Radiol Cardiothorac Imaging. 2021;3(1):e200484.

17. Wu FZ, Wu MT. 2014 SCCT guidelines for the interpretation and reporting of coronary CT angiography: a report of the Society of Cardiovascular Computed Tomography Guidelines Committee. J Cardiovasc Comput Tomogr. 2015;9(2):e3.

18. Cury RC, Leipsic J, Abbara S, Achenbach S, Berman D, Bittencourt M, et al. CAD-RADS 2.0 - 2022 Coronary Artery Disease-Reporting and Data System: An Expert Consensus Document of the Society of Cardiovascular Computed Tomography (SCCT), the American College of Cardiology (ACC), the American College of Radiology (ACR), and the North America Society of Cardiovascular Imaging (NASCI). JACC Cardiovasc Imaging. 2022;15(11):1974-2001.

19. Saraste A, Knuuti J. Evaluation of coronary artery disease after computed tomography angiography. Eur Heart J Cardiovasc Imaging. 2018;19(4):378-9.

20. Gueret P, Deux JF, Bonello L, Sarran A, Tron C, Christiaens L, et al. Diagnostic performance of computed tomography coronary angiography (from the Prospective National Multicenter Multivendor EVASCAN Study). Am J Cardiol. 2013;111(4):471-8.

21. Song YB, Arbab-Zadeh A, Matheson MB, Ostovaneh MR, Vavere AL, Dewey M, et al. Contemporary Discrepancies of Stenosis Assessment by Computed Tomography and Invasive Coronary Angiography. Circ Cardiovasc Imaging. 2019;12(2):e007720.

22. Arendt CT, Czwikla R, Lenga L, Wichmann JL, Albrecht MH, Booz C, et al. Improved coronary artery contrast enhancement using noise-optimised virtual monoenergetic imaging from dual-source dual-energy computed tomography. Eur J Radiol. 2020;122:108666.

23. Stehli J, Clerc OF, Fuchs TA, Possner M, Grani C, Benz DC, et al. Impact of monochromatic coronary computed tomography angiography from single-source dual-energy CT on coronary stenosis quantification. J Cardiovasc Comput Tomogr. 2016;10(2):135-40.

24. Gillies RJ, Kinahan PE, Hricak H. Radiomics: Images Are More than Pictures, They Are Data. Radiology. 2016;278(2):563-77.

25. Mayerhoefer ME, Materka A, Langs G, Haggstrom I, Szczypinski P, Gibbs P, et al. Introduction to Radiomics. J Nucl Med. 2020;61(4):488-95.

26. Euler A, Laqua FC, Cester D, Lohaus N, Sartoretti T, Pinto Dos Santos D, et al. Virtual Monoenergetic Images of Dual-Energy CT-Impact on Repeatability, Reproducibility, and Classification in Radiomics. Cancers (Basel). 2021;13(18).

27. Allmendinger T, Nowak T, Flohr T, Klotz E, Hagenauer J, Alkadhi H, et al. Photon-Counting Detector CT-Based Vascular Calcium Removal Algorithm: Assessment Using a Cardiac Motion Phantom. Invest Radiol. 2022;57(6):399-405.

28. Mergen V, Rusek S, Civaia F, Rossi P, Rajagopal R, Battig E, et al. Virtual calcium removal in calcified coronary arteries with photon-counting detector CT-first in-vivo experience. Front Cardiovasc Med. 2024;11:1367463.

29. Zsarnoczay E, Fink N, Schoepf UJ, O'Doherty J, Allmendinger T, Hagenauer J, et al. Ultra-high resolution photon-counting coronary CT angiography improves coronary stenosis quantification over a wide range of heart rates - A dynamic phantom study. Eur J Radiol. 2023;161:110746.

30. Hagar MT, Soschynski M, Saffar R, Rau A, Taron J, Weiss J, et al. Accuracy of Ultrahigh-Resolution Photon-counting CT for Detecting Coronary Artery Disease in a High-Risk Population. Radiology. 2023;307(5):e223305.

31. Halfmann MC, Bockius S, Emrich T, Hell M, Schoepf UJ, Laux GS, et al. Ultrahigh-Spatial-Resolution Photon-counting Detector CT Angiography of Coronary Artery Disease for Stenosis Assessment. Radiology. 2024;310(2):e231956.

32. Oostveen LJ, Boedeker KL, Brink M, Prokop M, de Lange F, Sechopoulos I. Physical evaluation of an ultra-high-resolution CT scanner. Eur Radiol. 2020;30(5):2552-60.

33. Moser LJ, Mergen V, Allmendinger T, Manka R, Eberhard M, Alkadhi H. A Novel Reconstruction Technique to Reduce Stair-Step Artifacts in Sequential Mode Coronary CT Angiography. Invest Radiol. 2024;59(9):622-8.

5 Danksagung

Zunächst möchte ich meinem Doktorvater, Prof. Dr. Karl-Friedrich Kreitner, sowie meinem Betreuer, Dr. Tilman Emrich, für die hervorragende Betreuung und ihre Unterstützung bei sämtlichen wissenschaftlichen Fragestellungen herzlich danken.

Mein besonderer Dank gilt zudem Dr. Moritz Halfmann, Prof. Dr. U. Joseph Schoepf, Prof. Dr. Dr. Akos Varga-Szemes und Prof. Dr. Michaela Hell für ihre fachliche Expertise und die Gelegenheit zur aktiven Mitarbeit an Forschungsprojekten.

Ich danke außerdem dem gesamten Team der Klinik und Poliklinik für Diagnostische und Interventionelle Radiologie der Universitätsmedizin Mainz für die stetige Begleitung, der Division of Cardiovascular Imaging der Medical University of South Carolina für die Ermöglichung meines Forschungsaufenthalts sowie dem Zentrum für Kardiologie in Mainz für die interdisziplinäre Zusammenarbeit im Rahmen des Forschungsprojekts.

Für die finanzielle Unterstützung danke ich der Studienstiftung des deutschen Volkes, dem Doktorandenstipendium des MAInz-DOC Promotionskollegs sowie dem Kaltenbach-Doktorandenstipendium der Deutschen Herzstiftung.

Abschließend danke ich meiner Familie und meinen Freunden von Herzen für ihren beständigen Rückhalt während der gesamten Promotionszeit.

6 Tabellarischer Lebenslauf